Complex of *Escherichia coli* Primary Replicative Helicase DnaB Protein with a Replication Fork: Recognition and Structure†

Maria J. Jezewska, Surendran Rajendran, and Wlodzimierz Bujalowski*

Department of Human Biological Chemistry and Genetics and The Sealy Center for Structural Biology, The University of Texas Medical Branch at Galveston, 301 University Boulevard, Galveston, Texas 77555-1053

Received October 15, 1997; Revised Manuscript Received December 4, 1997

ABSTRACT: Interactions of the *Escherichia coli* replicative helicase DnaB protein, with DNA replication fork substrates, have been studied using rigorous fluorescence titration, fluorescence energy transfer, and analytical ultracentrifugation methods. DnaB binds the 5′ single-arm fork, the 3′ single-arm fork, and the two-arm fork with stoichiometries of 1, 1, and 2 DnaB hexamers per fork, independent of the length of the duplex part of the fork. Within the structurally heterogeneous binding site, the helicase accesses most of the 20 nucleotide residues of an arm. The dsDNA of the fork does not contribute to the affinity; however, it affects the positioning of the enzyme on the 5′ or 3′ arm. Fluorescence energy transfer experiments provide direct evidence that the DnaB helicase binds the 5′ arm of the fork in a *single orientation*, with respect to the duplex part of the fork. The 33-kDa domains of the hexamer face the dsDNA, while the small 12-kDa domains face the 5′ end of the arm. In the complex with the 3′ arm, the helicase is bound in an opposite orientation when compared to the 5′ arm. *This is the first determination of the strict, single orientation of a helicase in the complex with a replication fork.* The 3′ arm accommodates a DnaB hexamer, while another hexamer is associated with the 5′ arm. The complex of two DnaB hexamers bound in opposite orientations with each arm of the fork may play an important role during bidirectional replication of the *E. coli* DNA.

Helicases are a class of enzymes that catalyze the unwinding of the duplex DNA in the processes of DNA replication, recombination, and repair and provide a metabolically active single-stranded intermediate. These enzymes are motor proteins that use the free energy of triphosphate hydrolysis to unwind dsDNA and to translocate along the nucleic acid lattice (*1, 2*).

DnaB is a key DNA replication protein in *Escherichia coli* and is involved in both the initiation and elongation stages of DNA replication (*2, 3*). The protein is the primary *E. coli* replicative helicase, i.e., the factor responsible for unwinding the duplex DNA in front of the replication fork during the chromosomal DNA replication, with preferential unwinding of dsDNA in the 5′ → 3′ direction (*3, 4*). The DnaB protein is the only helicase required to reconstitute DNA replication in vitro from the chromosomal origin of replication (oriC). The enzyme plays a crucial role in the replication of bacterial chromosomal, phage, and plasmid DNA (*2, 5*−*7*).

The DnaB helicase provides an outstanding model for the structure−function studies of a helicase. In the native form, DnaB exists as a hexamer composed of six identical subunits (*8*−*12*). Analytical sedimentation studies show that the DnaB helicase forms a stable hexamer over a large protein concentration range with magnesium cations playing a key role in stabilizing the hexameric structure (*9*−*12*). In fact, the strong stability of the DnaB hexamer distinguishes this enzyme from other well-studied hexameric helicases that exist in mixtures of various oligomeric forms (*13, 14*). Sedimentation data also show that the hexamer is the species which binds to ssDNA (*11*). Hydrodynamic and electron microscopy (EM)[1] data indicate that six protomers aggregate with cyclic symmetry. Thus, in the hexamer the protomer−protomer contacts are limited to only two neighboring subunits (*8, 15, 16*).

Using the quantitative fluorescence titration technique that eliminates any assumptions about the relationship between the observed signal change and the degree of binding, we recently characterized interactions of the DnaB helicase with ssDNA (*9*−*12, 17*). Rigorous analysis of the interactions was facilitated by the fact that binding of the DnaB protein to the ssDNA fluorescent derivative, poly(dεA), is accompanied by a strong increase of the nucleic acid fluorescence. We showed that in the stationary complex, in the presence of the ATP nonhydrolyzable analogue AMP-PNP, the DnaB hexamer binds polymer ssDNA with a site size of 20 ± 3 nucleotides per protein hexamer. Thermodynamic and photo-cross-linking studies showed that the DnaB hexamer has a single, strong binding site for ssDNA and that only a single subunit is primarily in contact with ssDNA

§ This work was supported by NIH Grant GM-46679 (to W.B.). The support of the John Sealy Memorial Endowment Fund 2545-95 and NIEHS Grant 5P30ES06676 is acknowledged. W.B. is a NIEHS Center Investigator.

* Corresponding author.

[1] Abbreviations: AMP-PNP, adenosine 5'-(β,γ-imidotriphosphate); Tris, tris(hydroxymethyl)aminomethane; EM, electron microscopy; CPM, 7-diethylamino-3-(4′-maleimidylphenyl)-4-methylcoumarin; FLM, fluorescein-5-maleimide; Hepes, *N*-(2-hydroxyethyl)piperazine-*N*′-2-ethanesulfonic acid; DEAE-cellulose, (diethylaminoethyl)cellulose; FITC, fluorescein 5′-isothiocyanate; CM, 7-diethylaminocoumarin-3-carboxylic acid, succimidyl ester.

S0006-2960(97)02564-6 CCC: $15.00
Published on Web 02/12/1998

(*17*). These results preclude the possibility of extensive wrapping of the ssDNA around the hexamer. The data also indicate that in the translocation of the enzyme along ssDNA a limited set of subunits, most probably only one, is engaged in the interactions with ssDNA at a time when the helicase interacts with the replication fork (*10, 11, 17, 18*).

Elucidation as to how a helicase interacts with a replication fork is of paramount importance for our understanding of the mechanism of the enzyme. In this paper, we report the quantitative analysis of the DnaB helicase−replication fork complex using the quantitative fluorescence titration technique, fluorescence energy transfer, and analytical sedimentation measurements. We provide direct evidence that, in the presence of the ATP nonhydrolyzable analogue AMP-PNP, the *E. coli* DnaB helicase can bind to both the 5′ and the 3′ arm of the replication fork, with a significant preference for the 5′ arm, independently of the length of the duplex part of the fork. In fact, the results show that the duplex part of the fork contributes little to the free energy of binding, although it affects the positioning of the enzyme bound to the arm. In the complex with the 5′ or 3′ arm, the helicase engages all 20 nucleotide residues of the arm; however, there is a strong heterogeneity in the interactions with ssDNA within the total DNA binding site of the helicase. The data indicate that the 3′ arm is not engaged in stable interactions with the helicase hexamer when it is bound in its stationary complex to the 5′ arm of the fork, thus leaving the 3′ arm fully accessible for the binding of the second DnaB hexamer. Fluorescence energy transfer data provide direct evidence that, with respect to the duplex part of the fork, the DnaB helicase binds the 5′ arm of the fork in a single orientation. The enzyme binds the 3′ arm in an opposite orientation as compared to the 5′ arm, which reflects the strict, single orientation of the helicase in the complex with ssDNA, with respect to the polarity of the sugar−phosphate backbone of the ss nucleic acid.

MATERIALS AND METHODS

Reagents and Buffers. All solutions were made with distilled and deionized >18 MΩ (Milli-Q Plus) water. All chemicals were reagent grade. Buffer T2 is 50 mM Tris adjusted to pH 8.1 with HCl, 5 mM $MgCl_2$, and 10% glycerol. The temperatures and concentrations of NaCl and AMP-PNP in the buffer are indicated in the text.

DnaB Protein. The *E. coli* DnaB protein was purified as previously described by us (*19*−*21*). The concentration of the protein was spectrophotometrically determined using the extinction coefficient $\epsilon_{280} = 1.85 \times 10^5$ cm^{-1} M^{-1} (hexamer) (*8*).

Nucleic Acids. All nucleic acids were purchased from Midland Certified Reagents (Midland, TX). The etheno derivatives of the nucleic acids were obtained by modification with chloroacetaldehyde or by direct synthesis using ϵA phosphoramidite (*17, 18, 22*). Single-stranded oligomers labeled at the 5′ end with fluorescein were synthesized using fluorescein phosphoramidite (Glen Research). Labeling of oligomers at the 3′ end with fluorescein and labeling at the 5′ or 3′ end with a coumarin derivative (CM) was performed by synthesizing the oligomers with the residue at the 5′ or 3′ end having the amino group on a six-carbon linker and, subsequently, modifying the amino group with FITC or CM. The degree of labeling was determined by the absorbance at 494 nm for fluorescein (pH 9) using the extinction coefficient $\epsilon = 7.6 \times 10^4$ M^{-1} cm^{-1} and at 437 nm for CM using the extinction coefficient $\epsilon = 4.43 \times 10^4$ M^{-1} cm^{-1} (*10*). Concentrations of all ssDNA oligomers have been spectrophotometrically determined using the nearest neighbor analysis (*11, 18, 23, 24*). The single-arm and the two-arm fork substrates were obtained by mixing the proper oligomers at given concentrations, warming up the mixture for 5 min at 95 °C, and slowly cooling for a period of ∼2 h (*18*).

Site-Directed Mutagenesis of the DnaB Helicase. Replacement of the arginine residues at position 14 from the N terminus of the DnaB protein and obtaining the DnaB protein variant (R14C) was performed using the plasmid harboring the gene of the wild-type DnaB helicase (*19*). The site-directed mutagenesis was accomplished in the NIEHS Center facility directed by Dr. T. Wood.

Labeling the DnaB R14C Variant with Fluorescent Markers. Labeling of the six cysteine residues of the DnaB variant (R14C hexamer) with CPM or FLM to obtain R14C−CPM and R14C−Fl was performed in H buffer (50 mM Hepes, pH 8.1, 100 mM NaCl, 5 mM $MgCl_2$, and 10% glycerol) at 4 °C. The fluorescent label was added from the stock solution to the molar ratio of the dye/R14C ≈ 25. The mixture was incubated for 4 h with gentle mixing. After incubation, the protein was precipitated with ammonium sulfate and dialyzed overnight against buffer T2. Any remaining free dye was removed from the modified R14C−CPM or R14C−Fl by applying the sample on a DEAE-cellulose column and eluting with buffer T2 containing 500 mM NaCl. The degree of labeling (γ) was determined by the absorbance of a marker using the extinction coefficient $\epsilon_{394} = 27 \times 10^3$ cm^{-1} M^{-1} for R14C−CPM and 78×10^3 cm^{-1} M^{-1} for R14C−Fl, respectively. The obtained values of γ were 5.8 ± 0.1 for CPM and 5.8 ± 0.1 for fluorescein, indicating that all cysteine residues in R14C are readily available for modification (Rajendran et al., manuscript in preparation).

Analytical Sedimentation Measurements. Sedimentation experiments were performed with the Optima XL-A analytical centrifuge using double-sector charcoal-filled 12-mm Epon centerpieces and sapphire windows. To read the homogeneously distributed sample, the solutions were scanned at the beginning of the run at the operational speed of 6000 rpm. The sedimentation was considered to be at equilibrium when consecutive scans, separated by time intervals of 8 h, did not indicate any changes. The baselines were determined by accelerating the samples to 60 000 rpm for 12 h and subsequently scanning the cells at the operational speed.

For a multicomponent system, the total concentration at radial position r is defined by (*8*)

$$c_r = \sum_{i=1}^{n} c_{bi} \exp\left\{\frac{[(1 - \bar{\nu}_i\rho)\omega^2 M_i(r^2 - r_b^2)]}{2RT}\right\} + b \quad (1)$$

where c_{bi}, $\bar{\nu}_i$, and M_i are the concentration at the bottom of the cell, partial specific volume, and molecular weight of the i component, respectively, ρ is the density of the solution, ω is the angular velocity, and b is the baseline error term. The analysis of the equilibrium sedimentation runs was performed as we previously described (*8, 9*). Equilibrium

sedimentation profiles were fitted to eq 1 with M_i and b as fitting parameters.

Fluorescence Measurements. All steady-state fluorescence measurements were performed using the SLM-AMINCO 48000S and 8100 spectrofluorometers (*25*). The emission spectra have been corrected for a wavelength dependence of the instrument response using software provided by the manufacturer. The binding of the DnaB protein was followed by monitoring the fluorescence of the etheno derivatives of ssDNA oligomers ($\lambda_{ex} = 325$ nm, $\lambda_{em} = 410$ nm). All titration points were corrected for dilution and, if necessary, for inner filter effect using the following formula (*19*)

$$F_{i\mathrm{cor}} = (F_i - B_i)\left(\frac{V_i}{V_o}\right)10^{0.5b(A_{i_{\lambda ex}})} \qquad (2)$$

where $F_{i\mathrm{cor}}$ is the corrected value of the fluorescence intensity at a given point of titration i, F_i is the experimentally measured fluorescence intensity, B_i is the background, V_i is the volume of the sample at a given titration point, V_o is the initial volume of the sample, b is the total length of the optical path in the cuvette expressed in centimeters, $A_{i_{\lambda ex}}$ is the absorbance of the sample at the excitation wavelength. Computer fits were performed using KaleidaGraph software (Synergy Software, PA) and Mathematica (Wolfram Research, IL). The relative fluorescence increase of the nucleic acid (ΔF) upon binding the DnaB protein is defined by

$$\Delta F = \frac{(F_{i\mathrm{cor}} - F_o)}{F_o} \qquad (3)$$

where $F_{i\mathrm{cor}}$ is the fluorescence of the nucleic acid solution at a given titration point i and F_o is the initial value of the fluorescence of the same solution.

All steady-state fluorescence anisotropy measurements were performed in the L format, using Glan−Thompson polarizers placed in the excitation and emission channels. The fluorescence anisotropy of the sample was calculated using (*26*)

$$r = \frac{(I_{VV} - GI_{VH})}{(I_{VV} - 2GI_{VH})} \qquad (4)$$

were I is the fluorescence intensity and the first and the second subscripts refer to vertical (V) polarization of the excitation and vertical (V) or horizontal (H) polarization of the emitted light (*20*). The factor $G = I_{HV}/I_{HH}$ corrects for the different sensitivity of the emission monochromator for vertically and horizontally polarized light (*27*). The limiting fluorescence anisotropies of fluorophores, r_o, were determined by measuring the anisotropy of a given sample at different solution viscosity, adjusted by sucrose or glycerol, and extrapolating to viscosity = ∞, using the Perrin equation (*26*).

Determination of the Average Fluorescence Energy Transfer Efficiency between Fluorophores on the Small Subunit of the DnaB Helicase and Fluorescent Labels Attached at Different Locations in the Replication Fork Substrates. The efficiencies of the radiationless energy transfer, E, between CPM (donor) and fluorescein (acceptor), located on the small 12-kDa domain of the DnaB protein variant R14C, and the fluorescein (acceptor) and CM (donor) placed at different locations of the 5′ and 3′ single-arm fork substrates in the complex with the helicase have been determined using two independent methods. The fluorescence of the donor in the presence of the acceptor (F_{DA}) is related to the fluorescence of the same donor (F_D) in the absence of the acceptor by

$$F_{DA} = (1 - \nu_D)F_D + F_D\nu_D(1 - E_D) \qquad (5a)$$

where ν_D is the fraction of donors in the complex with the acceptor and E_D is the average fluorescence energy transfer from donor to acceptor, determined from the quenching of the donor fluorescence. Thus, the average transfer efficiency (E_D) obtained from the quenching of the CPM fluorescence upon binding of the labeled ssDNA oligomer, is obtained by rearranging eq 5a as

$$E_D = \left(\frac{1}{\nu_D}\right)\left(\frac{F_D - F_{DA}}{F_D}\right) \qquad (5b)$$

The values of ν_D have been determined using the binding constants of the 20 and 10 mers for the DnaB helicase obtained in the same solution conditions (*10*).

In the second independent method, the average fluorescence transfer efficiency (E_A) has been determined using a sensitized acceptor fluorescence by measuring the fluorescence intensity of the acceptor (fluorescein) excited at 435 nm where the donor (CPM or CM) predominantly absorbs in the absence and presence of the donor. The fluorescence intensities of the acceptor in the absence (F_A) and in the presence (F_{AD}) of the donor are defined as

$$F_A = I_o\epsilon_A C_{AT}\phi_F^A \qquad (6a)$$

and

$$F_{AD} = (1 - \nu_A)F_A + I_o\epsilon_A\nu_A C_{AT}\phi_F^A + I_o\epsilon_D C_{DT}\phi_B^A E_A \qquad (6b)$$

where I_o is the intensity of incident light; C_{AT} and C_{DT} are the total concentrations of the acceptor and donor; ν_A is the fraction of acceptors in the complex with donors; ϵ_A and ϵ_D are the molar absorption coefficients of the acceptor and donor at the excitation wavelength (435 nm), respectively, ϕ_F^A and ϕ_B^A are the quantum yields of the free and bound acceptor, and E_A is the average transfer efficiency determined by a sensitized emission of the acceptor. All quantities in eqs 6a and 6b can be experimentally determined. For most of the cases considered in this work, the acceptor is practically completely saturated with the donor, i.e., $\nu_A \approx 1$. Therefore, for $\nu_A \approx 1$, dividing eq 6b by eq 6a and rearranging provides the average transfer efficiency described as

$$E_A = \left[\frac{1}{\nu_D}\right]\left(\frac{\epsilon_A C_{AT}}{\epsilon_D C_{DT}}\right)\left[\left(\frac{\phi_F^A}{\phi_B^A}\right)\left(\frac{F_{AD}}{F_A}\right) - 1\right] \qquad (7)$$

It should be pointed out that the energy transfer efficiencies (E_D and E_A) are apparent quantities. E_D is a fraction of the photons absent in the donor emission as a result of the presence of an acceptor, including transfer to the acceptor and possible nondipolar quenching processes induced by the presence of the acceptor; whereas, E_A is a fraction of all photons absorbed by the donor that were transferred to the

acceptor. The true Förster energy transfer efficiency (E) is a fraction of photons absorbed by the donor and transferred to the acceptor in the absence of any additional nondipolar quenching resulting from the presence of the acceptor (*26*). The value of E is related to the apparent quantities of E_D and E_A by (*28*)

$$E = \frac{E_A}{(1 + E_A - E_A)} \tag{8}$$

Therefore, measurements of the transfer efficiency, using both methods, are not alternatives but parts of the analysis to obtain the true efficiency of the fluorescence energy transfer process (E).

The fluorescence energy transfer efficiency between donor and acceptor dipoles is related to the distance (R) separating the dipoles by

$$E = \frac{R_o^6}{R_o^6 + R^6} \tag{9}$$

where $R_o = 9790\ (\kappa^2 n^{-4} \phi_d J)^{1/6}$ is the so-called Förster critical distance (in angstroms, Å), the distance at which the transfer efficiency is 50%; κ^2 is the orientation factor; ϕ_d is the donor quantum yield in the absence of the acceptor; and n is the refractive index of the medium ($n = 1.4$) (*26*). The overlap integral (J) characterizes the resonance between the donor and acceptor dipoles.

The fluorescence energy transfer in chemically identical donor and acceptor pairs, characterized by the same quantum yields, depends on the distance between the donor and acceptor (R) and the factor κ^2, describing the mutual orientation of the donor and acceptor dipoles (*26*). Although in the work presented in this paper, we are interested in relative distances between donors and acceptors, evaluation of κ^2 allowed us to estimate the effect of the orientation factor on the relative differences between the studied donor−acceptor distances. The factor κ^2 cannot be experimentally determined; however, the upper (κ^2_{max}) and lower (κ^2_{min}) limits of κ^2 can be obtained from the measured limiting anisotropies of the donor and acceptor and the calculated axial depolarization factors using the procedure described by Dale et al. (*29*). When both axial depolarization factors are positive, κ^2_{max} and κ^2_{min} can be calculated from $\kappa^2_{max} = (2/3)[1 + <d^X_D> + <d^X_A> + 3<d^X_D><d^X_A>]$ and $\kappa^2_{min} = (2/3)[1 - (1/2)(<d^X_D> + <d^X_A>)]$ where $<d^X_D>$ and $<d^X_A>$ are the axial depolarization factors for the donor and acceptor, respectively (*29*). The axial depolarization factors have been calculated as square roots of the ratios of the limiting anisotropies of the donors (CPM or CM) and the acceptor (fluorescein) and their corresponding fundamental anisotropies (*21*, *29*). For two chemically identical donor−acceptor pairs characterized by the same R_o (the same κ^2, ϕ_d, and J), the differences in the transfer efficiencies (E_1 and E_2) result exclusively from the different distances between the donor and acceptor, R_1 and R_2 (eq 9). The relative ratio of the two distances is then defined by

$$\frac{R_1}{R_2} = \left\{\frac{[(1 - E_1)E_2]}{[(1 - E_2)E_1]}\right\}^{1/6} \tag{10}$$

Determination of Rigorous Thermodynamic Binding Isotherms and True Stoichiometries of the DnaB Helicase Complexes with Fork Substrates. The binding of the DnaB protein to the fork substrates was followed by monitoring the fluorescence increase (ΔF) of their etheno derivatives upon the complex formation. A general procedure to obtain the true estimates of the average number of protein molecules bound per nucleic acid ($\sum \nu_i$) and the free protein concentration (P_F) has been previously described (*19*−*21*). This procedure is based on the fact that the experimentally observed ΔF, in the course of titration, is related to $\Sigma \nu_i$ by

$$\Delta F = \sum \nu_i \Delta F_{i\max} \tag{11}$$

where $\Delta F_{i\max}$ is the maximum fluorescence increase of nucleic acid with the DnaB protein bound in complex i. The value of $\Sigma \nu_i$ and P_F is then related to the total protein concentrations (P_{T_1} and P_{T_2}) and the total nucleic acid concentrations (N_{T_1} and N_{T_2}) at which the same ΔF is obtained by

$$\sum \nu_i = \frac{(P_{T_2} - P_{T_1})}{(N_{T_2} - N_{T_1})} \tag{12}$$

$$P_F = P_{T_x} - \sum \nu_i (N_{T_x}) \tag{13}$$

where $x = 1$ or 2 (*19*).

Analysis of the Binding of the DnaB Hexamer to Single-Arm Fork Substrates. As we show below, in the case of single-arm fork substrates, only one DnaB hexamer binds to the arm part of the fork. Therefore, binding of the DnaB helicase to single-arm fork substrates has been analyzed using a single-site binding isotherm as described by

$$\Delta F = \Delta F_{max}\left[\frac{KP_F}{(1 + KP_F)}\right] \tag{14}$$

where K is the binding constant characterizing the interactions of the helicase with the 5′ (K_1) or 3′ (K_2) single-arm fork, respectively, and ΔF_{max} is the maximum increase of the nucleic acid fluorescence at saturation with the enzyme.

THEORY

Analysis of the Binding of Two DnaB Hexamers to a Two-Arm Fork Having a Single-Arm Labeled with Ethenoadenosine. Consider a situation in which a two-arm fork can bind two DnaB hexamers with the binding sites located on the 5′ and 3′ arms of the fork, and only one arm, e.g., the 5′ arm, is labeled with ϵA (Figure 2a,b). Binding of the DnaB hexamers to the arms of the fork is characterized by the intrinsic binding constants K_1 (5′ arm) and K_2 (3′ arm). Because the binding sites (both arms) are very close to each other, we expect some interaction between the two large hexamers bound to the arms of the fork, even if the intrinsic binding affinities of the enzyme for each arm of the fork are not affected. These additional protein−protein interactions can be phenomenologically described by the parameter σ. The partition function (Z) describing the binding of the two DnaB hexamers to the two-arm fork is defined as

$$Z = 1 + (K_1 + K_2)P_F + K_1 K_2 \sigma P_F^2 \tag{15}$$

Let the fluorescence of the free 5′ arm be F_{F1} and the fluorescence of the 5′ arm with the DnaB protein bound, be F_{b1}. Then, the fluorescence (F) of the two-arm fork, labeled only at the 5′ arm, in the presence of the helicase is

$$F = F_{F1}N_F + F_{b1}K_1N_FP_F + F_{F1}K_2N_FP_F + F_{b1}K_1K_2\sigma N_FP_F^2 \quad (16)$$

The total nucleic acid concentration (N_T) is related to the free nucleic acid concentration (N_F) by the mass conservation equation

$$N_T = N_F(1 + K_1P_F + K_2P_F + K_1K_2\sigma P_F^2) \quad (17)$$

Introducing eq 17 into eq 16 and rearranging provides a theoretical equation relating the observed relative fluorescence increase (ΔF) to the binding of both hexamers to the two-arm fork

$$\Delta F = \frac{[\Delta F_1K_1P_F + \Delta F_1K_1K_2\sigma P_F^2]}{[Z]} \quad (18)$$

Equation 18 shows that the observed fluorescence increase of the nucleic acid sample upon titration with the protein results from the formation of the complex between the enzyme and the fluorescent arm and from the formation of the complex in which both protein molecules are bound. A series of theoretical titration curves of a replication fork labeled at only a single arm with different values of the cooperativity parameter (σ) is shown in Figure 1a. The maximum relative increase of fluorescence upon binding to the fluorescent 5′ arm is $\Delta F_{max} = 1.7$, and the affinities for the fluorescent 5′ arm and nonfluorescent 3′ arm are characterized by binding constants 3×10^7 and 3×10^6 M^{-1}, respectively. All curves reach the same plateau at saturation $\Delta F_{max} = 1.7$ for the studied range of σ values. However, at low values of σ, the maximum plateau is reached at higher protein concentrations. The decrease of σ, which reflects the increased negative cooperativity between the bound protein molecules, predominantly affects the upper part of the titration curve. This behavior results from the fact that the association process is initially dominated by the binding to the fluorescent 5′ arm. At higher protein concentrations, the contribution from the complex with two protein molecules bound becomes apparent (eq 18). Equation 18 shows that, for the very small values of σ, an apparent intermediate plateau of the titration curves should appear as

$$\Delta F_{max} \approx \Delta F_1\left[\frac{K_1}{(K_1 + K_2)}\right] \quad (19)$$

which is smaller by factor $K_1(K_1 + K_2)$ from the maximum value of $\Delta F_1 = 1.7$ characteristic for the binding of the protein to a 5′ arm alone (Figure 1a).

Analysis of the Binding of Two DnaB Hexamers to a Two-Arm Fork Having Both Arms Labeled with Ethenoadenosines. The analysis of the binding of the DnaB helicase to the replication fork substrate, where both arms are labeled with ethenoadenosines, is more complex than the analysis of the binding to a two-arm fork with only the 5′ arm labeled (discussed above). In this case, the fluorescence of the free 5′ arm and the 3′ arm are F_{F1} and F_{F2}, respectively, and the fluorescence of the 5′ arm and the 3′ arm associated with the DnaB protein are F_{b1} and F_{b2}. In the presence of the helicase, the fluorescence (F) of the two arm-fork is

$$F = (F_{F1} + F_{F2})N_F + (F_{b1} + F_{F2})K_1N_FP_F + (F_{F1} + F_{b2})K_2N_FP_F + (F_{b1} + F_{b2})K_1K_2\sigma N_FP_F^2 \quad (20)$$

Introducing mass conservation eq 17 into eq 20 provides the theoretical equation that relates the observed relative fluorescence increase (ΔF) to the binding of both DnaB hexamers to the two-arm fork, having both arms labeled with ϵA defined as

$$\Delta F = \frac{[(R_1\Delta F_1K_1 + R_2\Delta F_2K_2)P_F + (R_1\Delta F_1 + R_2\Delta F_2)K_1K_2\sigma P_F^2]}{[Z]} \quad (21)$$

where

$$\Delta F = \frac{[F - (F_{F1} + F_{F2})N_T]}{(F_{F1} + F_{F2})N_T} \quad (22a)$$

$$\Delta F_1 = \frac{(F_{b1} - F_{F1})}{F_{F1}} \quad (22b)$$

$$\Delta F_2 = \frac{(F_{b2} - F_{F2})}{F_{F2}} \quad (22c)$$

and

$$R_1 = \frac{F_{F1}}{(F_{F1} + F_{F2})} \quad (22d)$$

$$R_2 = \frac{F_{F2}}{(F_{F1} + F_{F2})} \quad (22e)$$

The quantities R_1 and R_2 are the contributions of each arm to the total fluorescence of the free two-arm fork; ΔF_1 and ΔF_2 are the relative increases of the fluorescence of the 5′ and 3′ arms, respectively, which are induced by protein binding; and Z is defined by eq 15. Figure 1b shows the theoretical titration curves of a two-arm fork substrate labeled on both arms with the protein for different values of the cooperativity factor (σ). The binding to the 5′ arm and the 3′ arm are characterized by the maximum fluorescence increase $\Delta F_1 = 1.7$ and $\Delta F_2 = 2.75$, and binding constants $K_1 = 3 \times 10^7$ M^{-1} and $K_2 = 3 \times 10^6$ M^{-1}, respectively. The system shows very characteristic behavior. For small values of σ, there is an intermediate plateau that is defined by

$$\Delta F \approx \left\{R_1\left[\frac{K_1}{(K_1 + K_2)}\right]\right\}\Delta F_1 + \left\{R_2\left[\frac{K_2}{(K_1 + K_2)}\right]\right\}\Delta F_2 \quad (23)$$

Thus, the intermediate plateau is at a lower value than ΔF_1 and ΔF_2, due to the weighting factors $\{R_1[K_1/(K_1 + K_2)]\}$ and $\{R_2[K_2/(K_1 + K_2)]\}$. The final plateau at saturation appears at $\Delta F = R_1\Delta F_1 + R_2\Delta F_2$.

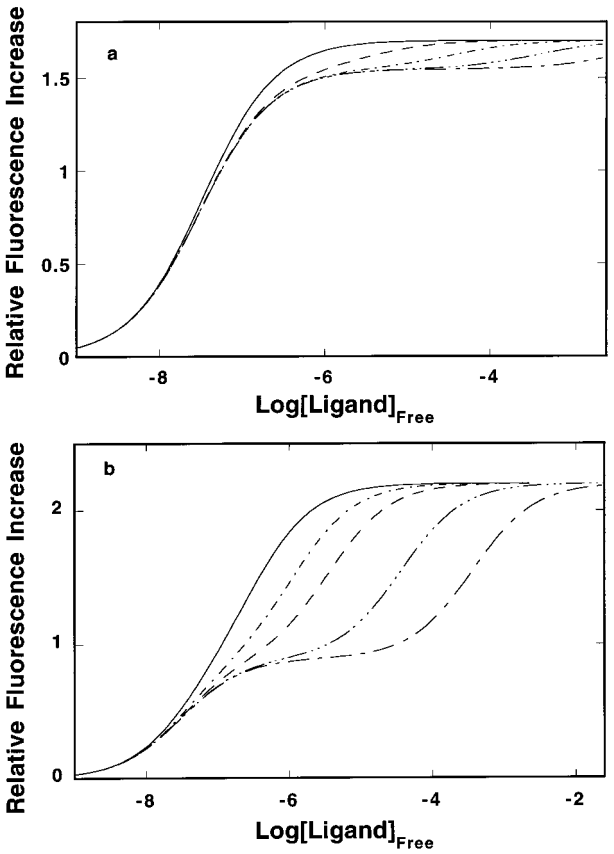

FIGURE 1: (a) Theoretical fluorescence titrations of a macromolecule having two different, discrete cooperative binding sites with the observed signal (fluorescence) originating only from the high-affinity site and characterized by the maximum relative increase, $\Delta F_{max} = 1.7$. The affinities for the binding sites are characterized by intrinsic binding constants, $K_1 = 3 \times 10^7$ M^{-1} and $K_2 = 3 \times 10^6$ M^{-1}, and different values of the cooperativity parameter σ: 1, (—); 10^{-1}, (— —); 10^{-2}, (— · —); 10^{-3}, (— ··· —); 10^{-4}, (— - —). (b) Theoretical fluorescence titrations of a macromolecule having two different, discrete cooperative binding sites with the observed signal (fluorescence) originating from both the high-affinity and low-affinity sites with the maximum relative increase of fluorescence $\Delta F_1 = 1.7$ and $\Delta F_2 = 2.75$, respectively (eqs 20−23). The affinities for the binding sites are characterized by intrinsic binding constants, $K_1 = 3 \times 10^7$ M^{-1} and $K_2 = 3 \times 10^6$ M^{-1}, and different values of the cooperativity parameter σ: 1, (—); 0.3, (— · —); 10^{-1}, (— —); 10^{-2}, (— ··· —); 10^{-3}, (— - —).

The analysis described above has been presented as applied to the binding of the DnaB helicase to the different replication fork substrates studied in this work. However, this analysis is general and applicable to any cooperative or noncooperative binding of a ligand to discrete binding sites on a macromolecule which differ in intrinsic spectroscopic (fluorescence in our case) and thermodynamic (binding constants, cooperativity) properties.

RESULTS

Binding of the DnaB Hexamer to Single-Arm Forks. Different DNA substrates, resembling the replication fork and used in the studies described in this work, are depicted in Figure 2a. The duplex part of each fork substrate is 20 bp long. Two of the substrates are single-arm forks, i.e., they have only one ssDNA extension, a 5′ or a 3′ arm. Each arm is a homooligonucleotide (dA) 20 bases long, which corresponds to the site size of the enzyme−ssDNA complex determined in studies with polymer ssDNA (*10*, *17*). In the middle of each arm there is a stretch of six fluorescent derivatives of adenosine (ethenoadenosines, ϵA) that provide the fluorescence signal to monitor the binding. A full two-arm fork (Figure 2a) has both arms containing the fluorescent ϵA. In subsequent studies, we used the fork substrates with a stretch of six ϵAs placed at different locations of the arms. The general structure of these substrates is illustrated in Figure 2b.

Fluorescence titrations of the 5′ single-arm fork, modified in the middle of the arm with six ϵAs (see Figure 2a), with the DnaB helicase at two different DNA concentrations in buffer T2 (pH 8.1, 10 °C) containing 100 mM NaCl and 1 mM AMP-PNP are shown in Figure 3a. Binding of the enzyme to the DNA is accompanied by a strong nucleic acid fluorescence increase, reflecting the interactions of the helicase with ϵA located in the arm (*18*). At saturation, the relative fluorescence increase reaches a maximum value of 1.7. Application of the general thermodynamic analysis of the ligand−macromolecule binding process (Materials and Methods) allows us to rigorously determine the stoichiometry of the complex. Figure 3b shows the dependence of the relative fluorescence increase (ΔF) as a function of the average number of the DnaB hexamers bound to the fork substrate. The true degree of binding of DnaB protein on the fork substrate could be determined, up to ~80% of the total binding isotherm. Short extrapolation to the maximum observed fluorescence signal shows the stoichiometry of 1.1 ± 0.1, thus, only a single DnaB hexamer binds to the 5′ single-arm fork at maximum saturation. The solid lines in Figure 3a are computer fits of the binding isotherms using eq 14, which provide the binding constant $K_1 = (1.7 \pm 0.3) \times 10^7$ M^{-1}.

Fluorescence titrations of the 3′ single-arm fork with the DnaB helicase in buffer T2 (pH 8.1, 10 °C) containing 100 mM NaCl and 1 mM AMP-PNP are shown in Figure 4a. Quantitative analysis of the binding isotherms (as described in Materials and Methods) shows that only one DnaB hexamer binds at saturation to the 3′ single-arm fork (Figure 4b). The solid lines in Figure 4a are computer fits of the binding isotherms using eq 14. The data show that the DnaB helicase binds the 3′ single-arm fork with significantly lower affinity as compared to the 5′ single-arm fork, with the binding process characterized by $K_2 = (2.5 \pm 0.5) \times 10^6$ M^{-1} (Figure 4a). Notice also that the maximum increase of the fluorescence of the 3′ single-arm fork upon saturation with the protein is higher ($\Delta F_{max} = 2.7$) than the $\Delta F_{max} = 1.7$ observed in the case of the 5′ single-arm DNA substrate (Figure 3a). These different values of the ΔF_{max} indicate that the enzyme induces different conformational changes in the nucleic acid in the complex with the 3′ arm as compared to the 5′ arm.

In the same solution conditions, the binding constant and the maximum fluorescence increase upon formation of the complex between the DnaB and the 20 mer (dA(pA)$_6$(pϵA)$_6$-(pA)$_7$), which is identical to the isolated arm of the studied fork substrates, are $K_{20} = (1.1 \pm 0.3) \times 10^7$ M^{-1} and $\Delta F_{max} = 1.7$, respectively (*18*). Thus, it is clear that the affinities of the helicase to the 20 mer and the 5′ single-arm fork (Figure 3a) are very similar, indicating that the duplex part of the fork does not significantly contribute to the free energy of the DnaB hexamer binding to the 5′ single-arm fork (*18*).

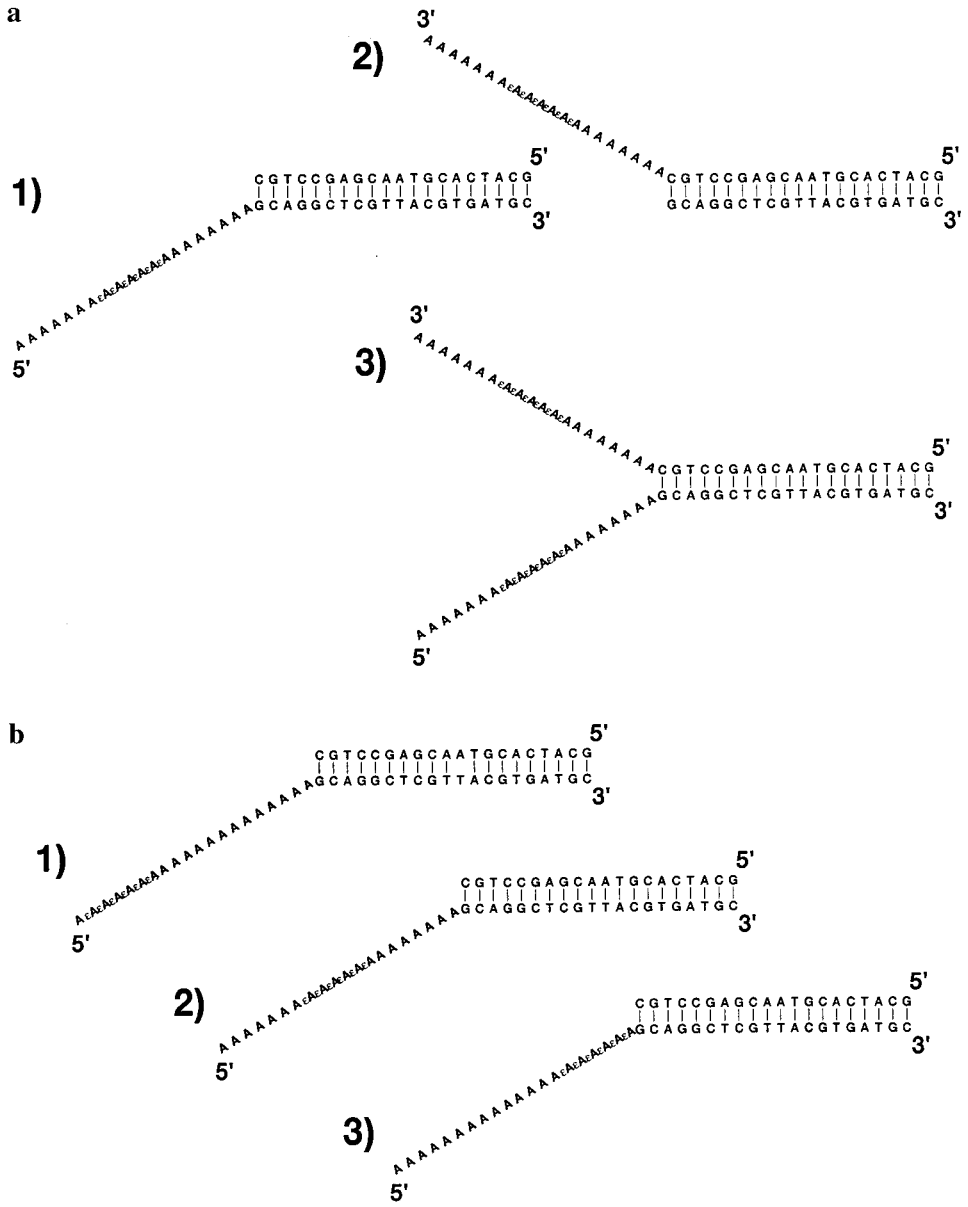

FIGURE 2: DNA substrates used in studying the interactions of the DnaB hexamer with the replication fork. (a) 1. The 5′ single-arm fork is constructed using a 40 mer, having at its 5′ end a track of 20 adenosine residues, with six middle residues replaced by ethenoadenosine (ϵA) fluorescent derivatives. The remaining 20 bases of the random sequence have been annealed to the complementary 20 mer, thus forming the duplex part of the fork 20 bp long. 2. The 3′ single-arm fork is constructed using an analogous 40 mer but having at its 3′ end a track of 20 adenosine residues, with six middle residues replaced by ϵA. 3. The full two-arm fork has been constructed by annealing the 40 mer, having at its 5′ end a track of 20 adenosine residues, with six middle residues replaced by ϵA. The remaining 20 bases of random sequence are complementary to 20 nucleotide residues of a corresponding 40 mer, which has at its 3′ end a track of 20 adenosine residues, with six middle residues replaced by ϵA. (b) The 5′ single-arm fork substrates in which a stretch of six ϵAs is placed in different locations on the arm of the fork: 1. at the 5′ end; 2. in the middle, and 3. at the duplex part. In analogous 3′ single-arm fork substrates, six ϵAs are placed at the same locations but along the 3′ arm of the fork.

On the other hand, a much lower affinity for the 3′ single-arm fork and a very different maximum fluorescence increase indicates that the duplex part of the fork plays a role in the binding process. Comparison between fluorescence titrations of the 5′ single-arm fork substrates, having 20 and 10 bp long duplex parts of the fork, with the DnaB helicase in buffer T2 (pH 8.1, 10 °C) containing 100 mM NaCl and 1 mM AMP-PNP is shown Figure 5a. Analogous titrations of the 3′ single-arm fork substrates having 20 and 10 bp long duplex parts of the fork are shown in Figure 5b. The quantum yields of the free nucleic acids with 20 and 10 bp long duplex parts are, within experimental accuracy, the same. The affinity of the enzyme is only slightly affected by the different lengths of the duplex part. However, the maximum fluorescence increase of the nucleic acid fluorescence is significantly different, decreasing from 1.7 to 1.2 and from 2.7 to 1.2 in the case of the 5′ and 3′ single-arm forks, respectively (*18*). Therefore, the data suggest that while the duplex part of the fork does not contribute to the free energy of binding it is affecting the positioning of the helicase bound to the 5′ or 3′ arm, i.e., changing the effect of the enzyme on the conformation of the ssDNA in the binding site.

The lower affinity and the different ΔF_{max} accompanying the binding of the helicase to the 3′ arm suggest that the enzyme associates with this fork substrate in a different

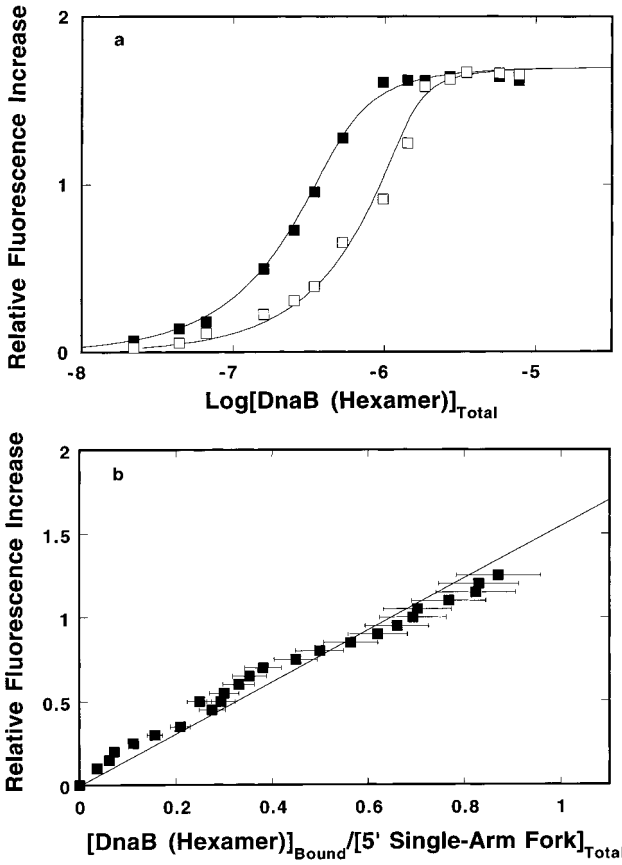

FIGURE 3: (a) Fluorescence titrations of the 5′ single-arm fork, having six ϵAs in the middle of the arm, with the DnaB protein (λ_{ex} = 325 nm, λ_{em} = 410 nm) in buffer T2 (pH 8.1, 10 °C) containing 100 mM NaCl and 1 mM AMP-PNP at two different nucleic acid concentrations: (■) 4.5×10^{-7} M; (□) 1.45×10^{-6} M (fork). Solid lines are computer fits of the titration curves, using a single-site binding isotherm, with intrinsic binding constant $K_1 = 1.7 \times 10^7$ M^{-1} and relative fluorescence change $\Delta F_1 = \Delta F_{max} = 1.7$ (eq 14). (b) Dependence of the relative fluorescence of the fork substrate, ΔF, upon the average number of bound DnaB hexamers (■). The solid line follows the experimental points from 0 to $\Delta F_{max} = 1.7$ and has no theoretical basis. Error bars are standard deviations obtained using 4−5 titrations.

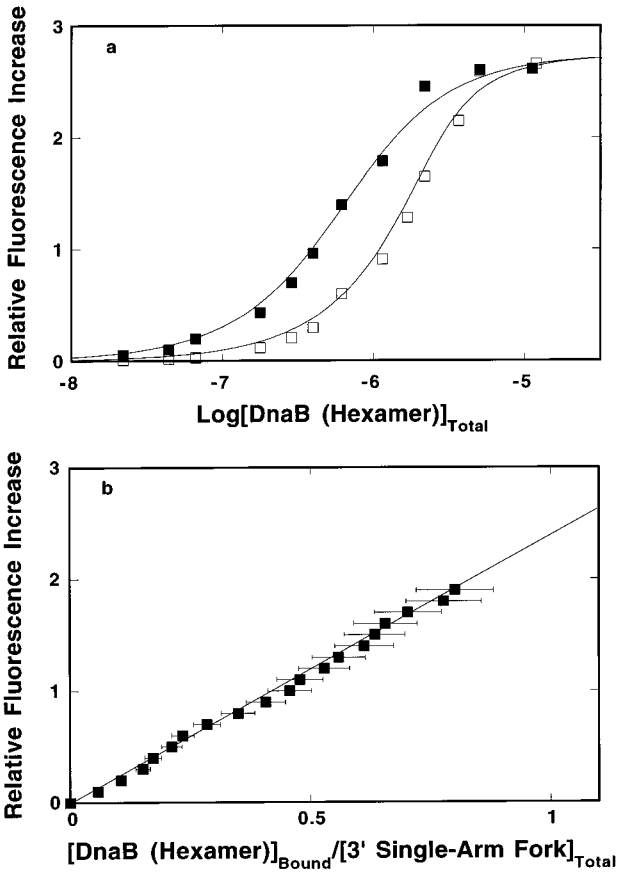

FIGURE 4: (a) Fluorescence titrations of the 3′ single-arm fork, having six ϵAs in the middle of the arm, with the DnaB protein (λ_{ex} = 325 nm, λ_{em} = 410 nm) in buffer T2 (pH 8.1, 10 °C) containing 100 mM NaCl and 1 mM AMP-PNP at two different nucleic acid concentrations: (■) 4.5×10^{-7} M; (□) 1.45×10^{-6} M (fork). Solid lines are computer fits of the titration curves, using a single-site binding isotherm, with intrinsic binding constant $K_2 = 2.5 \times 10^6$ M^{-1} and relative fluorescence change $\Delta F_2 = \Delta F_{max} = 2.75$ (eq 14). (b) Dependence of the relative fluorescence of the fork substrate, ΔF, upon the average number of bound DnaB hexamers (■). The solid line follows the experimental points from 0 to $\Delta F_{max} = 2.75$ and has no theoretical basis. Error bars are standard deviations obtained using 4−5 titrations.

orientation, with respect to the duplex part of the fork, than in the complex with the 5′ single-arm fork (*18*). Such a different orientation would make the accommodation of the duplex DNA more difficult in the case of the 3′ arm, leading to a lower affinity and a different fluorescence change, reflecting changes in the interactions of the enzyme with ssDNA in the arm. Fluorescence energy transfer experiments described below show that the enzyme indeed binds the 3′ arm in an opposite orientation than the 5′ arm (see below and Discussion).

Binding of the DnaB Hexamer to Two-Arm Fork Substrates. The role of both arms, in interactions with the helicase, can be determined by studying the binding of the enzyme to the full two-arm fork substrate. In the first set of experiments, we performed binding studies of the DnaB helicase to the two-arm replication fork substrate, labeled in the middle of both 5′ and 3′ arms with six ϵA, as depicted in Figure 2a. Fluorescent titrations of the full two-arm fork at two different concentrations of the nucleic acid are shown in Figure 6a. There is a dramatic difference between these titrations and the binding curves obtained for the single-arm forks. While in the studied solution conditions, only a single binding phase is observed in the case of the 5′ and 3′ single-arm fork substrates, a biphasic character of the isotherms is evident in the titrations of the two-arm fork labeled on both arms with ϵA, particularly at a lower nucleic acid concentration (Figure 6a). There is a strong-affinity step with a plateau around $\Delta F \approx 0.8$ followed by a low-affinity step with a plateau around $\Delta F \approx 2.2$ (*18*). The average number of DnaB hexamers bound per two-arm fork has been determined by using the thermodynamically rigorous method (Materials and Methods). The dependence of the relative fluorescence increase as a function of the number of DnaB hexamers bound to the fork substrate is shown in Figure 6b. These data show that at the first plateau ($\Delta F \sim 0.8$) only one DnaB hexamer binds to the two-arm fork followed by the binding of the second hexamer in the second phase of the isotherm. These results have been subsequently confirmed by analytical centrifugation experiments (see below). The plot is nonlinear, reflecting the large difference in the ΔF accompanying the binding in the first and second steps. These data show that the two-arm fork can bind two DnaB hexamers with each single hexamer bound to a single arm of the fork.

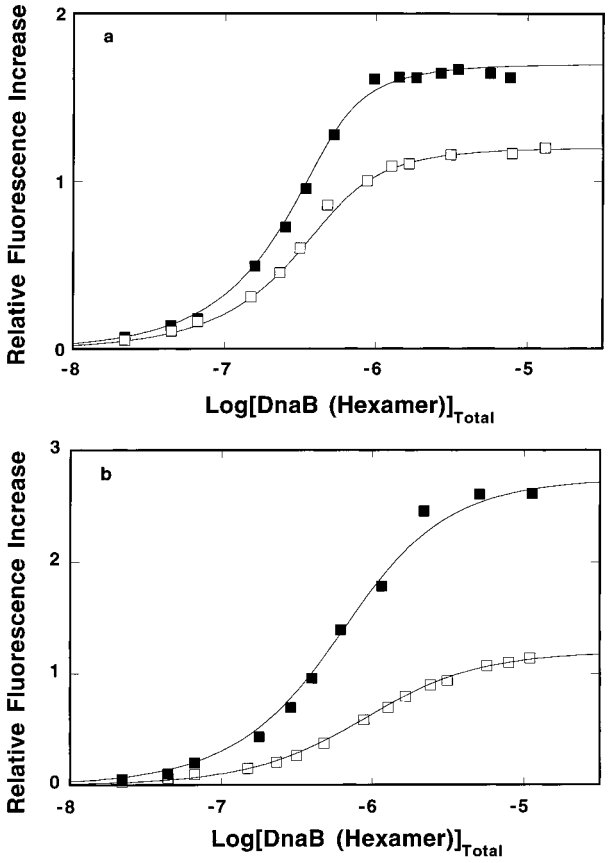

FIGURE 5: (a) Fluorescence titrations of 5′ single-arm forks having six ϵAs in the middle of the arm and differing in the number of base pairs in the duplex parts of the fork, with the DnaB protein (λ_{ex} = 325 nm, λ_{em} = 410 nm) in buffer T2 (pH 8.1, 10 °C) containing 100 mM NaCl and 1 mM AMP-PNP: (■) 20 bp; (□) 10 bp. The nucleic acid concentrations are 4.5×10^{-7} M (fork) in both cases. Solid lines are the computer fits of a single-site binding isotherm (eq 14) with intrinsic binding constants $K_1 = 1.7 \times 10^7$ M^{-1}; $\Delta F_1 = 1.7$; $K_1 = 1 \times 10^7$ M^{-1}; $\Delta F_1 = 1.2$. (b) Fluorescence titrations of 3′ single-arm forks having six ϵA in the middle of the arm and differing in the number of base pairs in the duplex parts of the fork, with the DnaB protein (λ_{ex} = 325 nm, λ_{em} = 410 nm) in buffer T2 (pH 8.1, 10 °C) containing 100 mM NaCl and 1 mM AMP-PNP: (■) 20 bp; (□) 10 bp. The nucleic acid concentrations are 4.5×10^{-7} M (fork) in both cases. Solid lines are the computer fits of single-binding site isotherms (eq 14) with intrinsic binding constants $K_2 = 2.5 \times 10^6$ M^{-1}; $\Delta F_2 = 2.75$; $K_2 = 1.5 \times 10^6$ M^{-1}; $\Delta F_2 = 1.2$.

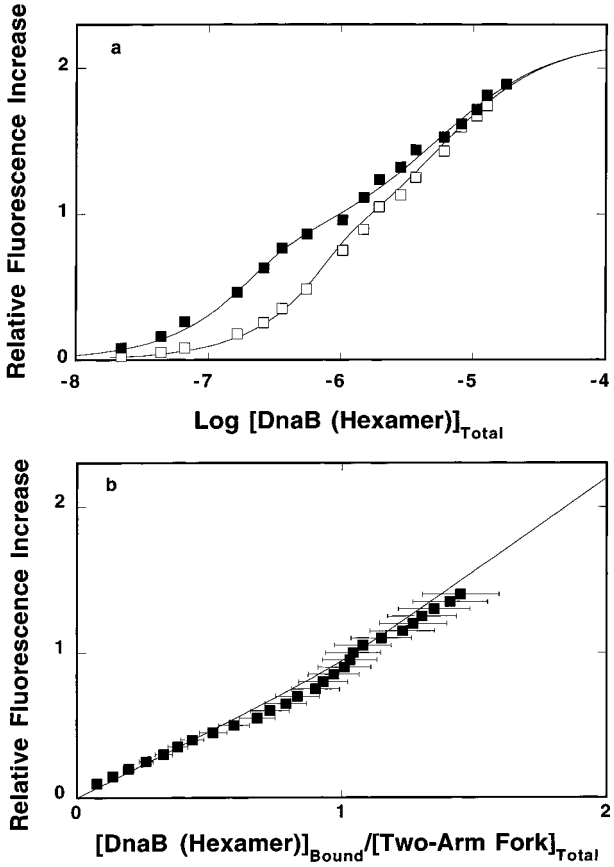

FIGURE 6: (a) Fluorescence titrations of the two-arm fork, having a 20 bp long duplex part and both arms labeled with six ϵAs in the middle of each arm, with the DnaB protein (λ_{ex} = 325 nm, λ_{em} = 410 nm) in buffer T2 (pH 8.1, 10 °C) containing 100 mM NaCl and 1 mM AMP-PNP at two different nucleic acid concentrations: (■) 2.2×10^{-7} M (fork); (□) 9×10^{-7} M (fork). Solid lines are the computer fits using a two-site binding isotherm (eq 21) with intrinsic binding constants $K_1 = 1.7 \times 10^7$ M^{-1}; $\Delta F_1 = 1.7$; $K_2 = 2.5 \times 10^6$ M^{-1}; $\Delta F_2 = 2.75$; and $\sigma = 0.08$. The fractional contribution of each arm to total intensity of the two-arm fork, $R_1 = 0.5$ and $R_2 = 0.5$, were determined from the comparison of the quantum yield of the full two-arm fork and the corresponding single-arm forks in the absence of the helicase. (b) Dependence of the relative fluorescence increase, ΔF, upon the average number of DnaB helicase hexamers bound per fork (■). Error bars are standard deviations obtained using 4−5 titrations. Solid line is the theoretical dependence of ΔF upon the average number of bound DnaB hexamers per fork at a given fork concentration, as defined by eq 21.

Thermodynamic studies described above show that the binding of the helicase to the 5′ single-arm fork has a significantly higher affinity than the affinity for the 3′ arm and that the relative fluorescence change accompanying the binding to the 5′ single arm is lower than the fluorescence change accompanying the association of the enzyme with the 3′ single-arm (Figures 3a and 4a). In this context, it should be pointed out that the macroscopic affinity of the first binding phase coincides exactly with the affinity of the helicase for the 5′ single-arm. Also, the relative fluorescence change of the high affinity phase of the binding isotherm of the two-arm fork is lower (∼0.8) as compared to the relative fluorescence change of ∼1.4 accompanying the binding in the low-affinity step. Thus, the obtained results indicate that the high-affinity step corresponds to the binding of the DnaB hexamer to the 5′ arm of the two-arm fork and the low-affinity step reflects the binding of the enzyme to the 3′ arm of the two-arm fork (*18*).

The fact that two DnaB hexamers can bind to a two-arm fork with each hexamer associated with a single arm of the fork indicates that the 3′ arm is available for the DnaB protein to bind, even when the first DnaB hexamer is already associated with the 5′ arm. The extent to which the presence of the two arms affects the binding of the enzyme to the fork substrate can be estimated by comparing the affinity of the helicase for the single-arm forks to the binding of the enzyme to the DNA substrate where both arms are present. In other words, we want to know to what extent binding of the two DnaB hexamers reflects independent binding of a single hexamer to a single arm of the fork. There are two simple alternative models that can be considered. In the first model, the hexamers bind with the same intrinsic affinities and with the same relative changes of the fluorescence as to the single-arm forks. Because two large DnaB hexamers are simultaneously bound to the fork, any additional free

energy changes in the binding process result from protein−protein interactions due to the close proximity of the hexamers. The behavior of this model is described by eqs 20−23 and illustrated in Figure 1b. In the second model, simultaneous binding of both hexamers to the two-arm fork affects the interactions of each hexamer with a corresponding arm. In this model, the hexamers would not form the same complexes with the arms of the fork, as in the case of the single-arm forks. As a result, the binding would occur with different intrinsic affinities and also with different fluorescence changes when compared to the single-arm forks.

Because the binding in the high-affinity phase to the two-arm fork occurs in the same concentration range of the protein as the binding to the 5′ single-arm fork, the data indicate that the affinity to the 5′ arm is not affected by the presence of the 3′ arm. Moreover, the intermediate and final plateaus occur at $\Delta F \approx 0.8$ and ≈ 2.2, respectively, as predicted by eqs 20−23, if the fluorescence changes accompanying the binding of the helicase to both arms are exactly the same as the fluorescence changes accompanying the association with the 5′ and 3′ single-arm forks. Therefore, these data indicate that intrinsic affinities, as well as the fluorescence changes accompanying the binding to each arm of the fork, are not affected by the simultaneous binding of both hexamers to a two-arm fork and strongly support the first model, as defined by eqs 20−23.

Fluorescence titrations with single-arm substrates provide the intrinsic affinities of the DnaB hexamer for the 5′ and 3′ arms of the fork, characterized by binding constants (K_1 and K_2) and the corresponding relative fluorescence increases, (ΔF_1 and ΔF_2) (eq 20−23). The simultaneous binding of the two hexamers to the full two-arm fork is then described by the same binding constants (K_1 and K_2) and the relative fluorescence increases (ΔF_1 and ΔF_2) as obtained from titrations with the single-arm forks. The additional possible interactions resulting from the very close proximity of both large hexamers bound to the fork are then characterized by factor σ. There are five parameters in eq 21; however, four parameters are independently determined in the titrations with single-arm forks.

The solid lines in Figure 6a are the computer simulations of the binding of two DnaB hexamers to the full two-arm replication fork using K_1, K_2, ΔF_1, and ΔF_2 as obtained from the titrations with single-arm forks (eq 21). The only fitted parameter that reflects additional interactions between the hexamers brought to close proximity when bound to the arms of the fork is $\sigma = 0.08$. It is evident that the model precisely reproduces the experimental biphasic isotherm. Thus, each arm in the two-arm fork can bind a single DnaB hexamer with the same intrinsic affinity, as in the case of single-arm forks, with additional protein−protein interactions resulting from the close proximity of the two hexamers in the complex.

In the case of binding of the DnaB helicase to a two-arm fork with only a single arm labeled (Figure 2a), the observed signal originates from the association of the enzyme with the labeled arm while the other arm is spectroscopically "silent". Such a situation is described by eq 18 and illustrated in Figure 1a. Fluorescent titrations of the two-arm fork substrate labeled in the middle of its 5′ arm with six ϵAs, with the helicase in buffer T2 (pH 8.1, 10 °C) containing 100 mM NaCl and 1 mM AMP-PNP at two different concentrations of the nucleic acid are shown in

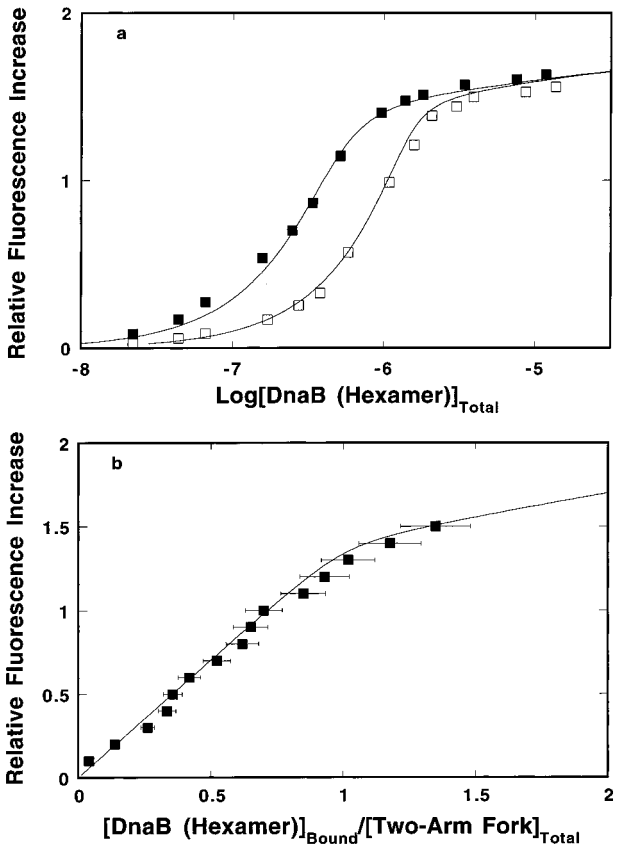

FIGURE 7: (a) Fluorescence titrations of the two-arm fork, having a 20 bp long duplex part and only the single 5′ arm labeled with six ϵAs in the middle of the arm, with the DnaB protein (λ_{ex} = 325 nm, λ_{em} = 410 nm) in buffer T2 (pH 8.1, 10 °C) containing 100 mM NaCl and 1 mM AMP-PNP at two different nucleic acid concentrations: (■) 4.5×10^{-7} M (fork); (□) 1.45×10^{-6} M (fork). Solid lines are the computer fits of a two-site binding isotherm (eq 18) with intrinsic binding constants $K_1 = 1.7 \times 10^7$ M^{-1}; $\Delta F_1 = 1.7$; $K_2 = 2 \times 10^6$ M^{-1}; and $\sigma = 0.05$. (b) Dependence of the relative fluorescence increase, ΔF, upon the average number of DnaB helicase hexamers bound per fork (■). Solid line is the theoretical dependence of ΔF upon the average number of bound DnaB hexamers per fork substrate, as defined by eq 18. Error bars are standard deviations obtained using 4−5 titrations.

Figure 7a. The maximum plateau of the titration curves reaches the same value of $\Delta F_{max} = 1.7$ as in the case of the 5′ single-arm fork substrate, although the plateau is reached at much higher concentrations of the enzyme. Moreover, only an apparent single binding phase is observed. Figure 7b shows the dependence of the relative fluorescence increase upon the average number of DnaB hexamers bound to the fork. Clearly, the plot is nonlinear with ∼85% of the fluorescence change occurring upon binding of the single hexamer. Because the observed signal originates from the binding to the 5′ arm (single, fluorescent binding site), the binding isotherms are described by eq 18. There are four parameters (K_1, K_2, σ, and ΔF_1) describing the binding isotherms but only two parameters (K_1 and ΔF_1) are known from the titrations with the single-arm fork. Thus, contrary to the two-arm fork where both arms are labeled, there are two parameters (K_2 and σ) that must be fitted. Solid lines in Figure 7a are computer fits of the binding isotherms that provide $K_2 = (2 \pm 0.5) \times 10^6$ M^{-1} and $\sigma = 0.05 \pm 0.02$. These values are in excellent agreement with the corresponding values obtained from titrations with single-arm fork

substrates and the two-arm fork labeled at both arms with ϵA (Figures 3a, 4a, and 6a). Notice that the nonfluorescent 3′ arm of the fork substrate is slightly different from the fluorescent 5′ arm by the presence of six unmodified adenosine residues. The similar values of K_2 for both arms reflect similar binding constants of the DnaB helicase to the ssDNA oligomers, which are composed of different bases (*10*).

Binding of the DnaB Helicase to Replication Fork Substrates Modified with ϵA at Different Locations of the Arms. To obtain information about how different parts of the arms are engaged in interactions with the enzyme, we performed binding studies with fork substrates having arms modified with six ϵAs at different locations of the arms (Figure 2b). Fluorescence titrations of the 5′ single-arm fork substrate with a stretch of six ϵAs located at the 5′ end, in the middle, and in the direct vicinity of the duplex part of the DNA substrate with the DnaB helicase in buffer T2 (pH 8.1, 10 °C) containing 100 mM NaCl and 1 mM AMP-PNP are shown in Figure 8a. Although the affinities for the fork substrates with ϵAs in different locations in the arm are very similar (Table 1), there are significant differences between the relative maximum increases of the nucleic acid fluorescence (ΔF_{max}) upon saturation with the enzyme. The highest increase of the fluorescence ($\Delta F_{max} = 1.7$) is observed in the case of the fork substrate modified with ϵA in the middle of the arm, indicating that the structure of the ssDNA is affected the most by the helicase in this region on the arm. A slightly lower increase of the nucleic acid fluorescence occurs when the arm of the fork is modified at its 5′ end with $\Delta F_{max} = 1.4$, thus strongly suggesting that this region of the arm is also fully engaged in interactions with the enzyme. The strikingly low fluorescence increase is observed for the fork substrate with six ϵAs located close to the duplex DNA ($\Delta F_{max} = 0.45$). This low fluorescence increase indicates that the interactions of the helicase with this part of the arm are very different from interactions with the rest of the arm. The increase of the ϵA fluorescence in a polymer nucleic acid reflects conformational changes of the DNA, most probably leading to stronger separation and immobilization of the ethenoadenosine residues. The obtained results indicate that the helicase induces less pronounced conformational changes in the ssDNA in close proximity to the duplex DNA of the fork, suggesting much weaker interactions with ssDNA in this region of the arm within the active site of the enzyme (see Discussion).

Fluorescence titrations of the 3′ single-arm fork substrate with a stretch of six ϵAs located at the 3′ end, in the middle, and in the direct vicinity of the duplex part of the DNA substrate with the DnaB helicase in buffer T2 (pH 8.1, 10 °C) containing 100 mM NaCl and 1 mM AMP-PNP are shown in Figure 8b. As in the case of the 5′ arm, the affinities of the enzyme for the DNA substrates with ϵA placed in different locations on the arm are very similar (Table 1), with the large differences occurring to the extent of the nucleic acid fluorescence increase upon saturation with the protein. The highest increase of the nucleic acid fluorescence is observed when the ϵAs are located in the middle of the 3′ arm ($\Delta F_{max} = 2.7$), indicating that this part of the arm is predominantly affected by the bound enzyme. Significantly lower increases of the nucleic acid fluorescence are observed for the ϵA located at the 3′ end and at the duplex part of the DNA substrate and characterized by $\Delta F_{max} =$ 1.0 ± 0.1 and $= 0.9 \pm 0.1$, respectively. The fact that the helicase affects the fluorescence of the ϵA placed in very different locations of the arm indicates that, similar to the 5′ single-arm fork, the enzyme accesses the whole 3′ arm of the DNA substrate. However, quantitatively, the effect of the enzyme on the nucleic acid conformation is different than that observed for the analogous 5′ single-arm fork substrates. This difference most probably results from a different orientation of the helicase when bound to the 3′ arm as compared to 5′ arm (see below).

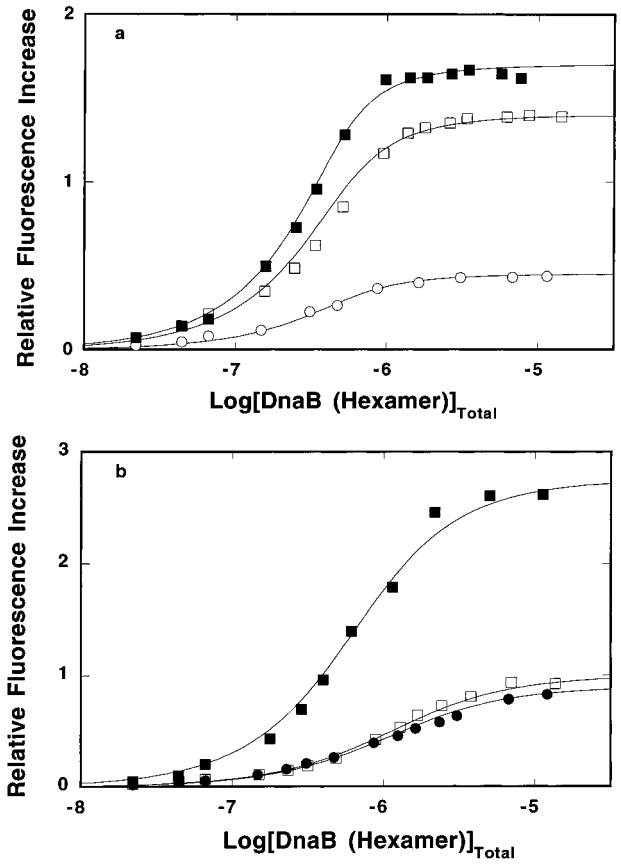

FIGURE 8: (a) Fluorescence titrations of the 5′ single-arm fork, labeled with six ϵAs at its 5′ end, in the middle of the arm, and adjacent to the 20 bp long duplex part of the fork, with the DnaB protein ($\lambda_{ex} = 325$ nm, $\lambda_{em} = 410$ nm) in buffer T2 (pH 8.1, 10 °C) containing 100 mM NaCl and 1 mM AMP-PNP: (□) six ϵA at the 5′ end; (■) six ϵAs the middle of the arm; (○) six ϵAs adjacent to the duplex part of the fork (Figure 2b). The concentrations of the nucleic acids are 4.5×10^{-7} M (fork). Solid lines are the computer fits using a single-site binding isotherm (eq 14) with intrinsic binding constants K_1 and relative fluorescence increase, ΔF_1: $K_1 = 1 \times 10^7$ M^{-1}, $\Delta F_1 = 1.4$; $K_1 = 1.7 \times 10^7$ M^{-1}, $\Delta F_1 = 1.7$; $K_1 = 8 \times 10^6$ M^{-1}, $\Delta F_1 = 0.45$. (b) Fluorescence titrations of the 3′ single-arm fork, labeled with six ϵA at its 3′ end, in the middle of the arm, and adjacent to the 20 bp long duplex part of the fork, with the DnaB protein ($\lambda_{ex} = 325$ nm, $\lambda_{em} = 410$ nm) in buffer T2 (pH 8.1, 10 °C) containing 100 mM NaCl and 1 mM AMP-PNP: (□) 3′ end labeled with six ϵAs; (■) six ϵAs in the middle of the arm; (●) six ϵAs adjacent to the duplex part of the fork. The nucleic acid concentrations are 4.5×10^{-7} M (fork). Solid lines are the computer fits of a single-site binding isotherm (eq 14) with intrinsic binding constants $K_2 = 1.1 \times 10^6$ M^{-1}, $\Delta F_2 = 1$; $K_2 = 2.5 \times 10^6$ M^{-1}, $\Delta F_2 = 2.75$; $K_2 = 1.2 \times 10^6$ M^{-1}, $\Delta F_2 = 0.9$.

Analytical Sedimentation Studies of the Complexes of the DnaB Hexamer with Replication Fork Substrates. Analytical equilibrium sedimentation studies have been performed with replication fork substrates that have a 20 bp long duplex part

Table 1: Thermodynamic and Fluorescence Parameters of Complexes of 5′ Single-arm Substrates and 3′ Single-Arm Substrates, Labeled with Six ϵAs at the End, in the Middle, and at the Duplex Part of the Fork (Figure 2b), with the DnaB Helicase in Buffer T2 (pH 8.1, 10 °C) Containing 100 mM NaCl and 1 mM AMP-PNP; $\lambda_{ex} = 325$ Nm, $\lambda_{em} = 410$ nm

	5′ single-arm fork		3′ single-arm fork	
	K (M^{-1})	ΔF_{max}	K (M^{-1})	ΔF_{max}
ϵA at the end of the arm	$(1 \pm 0.3) \times 10^7$	1.4 ± 0.2	$(1.2 \pm 0.3) \times 10^6$	1.2 ± 0.2
ϵA in the middle	$(1.7 \pm 0.3) \times 10^7$	1.7 ± 0.2	$(2.5 \pm 0.3) \times 10^6$	2.7 ± 0.2
ϵA at the duplex part	$(8 \pm 3) \times 10^6$	0.5 ± 0.1	$(1.1 \pm 0.4) \times 10^6$	1.2 ± 0.2

of the fork, analogous to the substrates depicted in Figure 2a, but with unmodified adenosine residues instead of ϵA. The nucleic acids have been labeled with CM through a six-carbon amino linker at the 5′ ends of the duplex part of the forks. This approach allowed us to monitor exclusively the complex between the helicase and the DNA without interference from protein and AMP-PNP absorbances.

A concentration profile of the DnaB helicase complex with the 3′ single-arm fork as a function of the square of the radius at sedimentation equilibrium in buffer T2 (pH 8.1, 10 °C) containing 100 mM NaCl and 1 mM AMP-PNP is shown in Figure 9a. The DnaB concentration is 1×10^{-5} M (hexamer), and the nucleic acid is 1×10^{-6} M (fork), thus the helicase is in large molar excess over the nucleic acid ensuring complete saturation of the fork. The solid line is a nonlinear least-squares fit to a single exponential function (eq 1). Including an extra exponential term does not cause significant improvement of the fit. The excellent agreement between the theoretical line and the experimentally obtained concentration profile indicates that there is a single species in solution. The analysis of the concentration profiles provides the molecular weight of 355 000 ± 20 000. Similar values were obtained for higher (up to $\sim 2 \times 10^{-5}$ M) concentrations of the protein (data not shown). Since the molecular weights of the DnaB hexamer and fork are ∼ 314 000 and ∼ 25 000, the obtained data show that at saturation the DnaB helicase forms a 1:1 complex with the 3′ single-arm fork substrate. Virtually the same result has been obtained in the case of the complex of the DnaB helicase with the 5′ single-arm fork substrate (data not shown).

A different behavior is observed in the case the two-arm fork. A concentration profile of the complex of the DnaB helicase with the two-arm fork monitored at 437 nm as a function of the square of the radius at sedimentation equilibrium in buffer T2 (pH 8.1, 10 °C) containing 100 mM NaCl and 1 mM AMP-PNP is shown in Figure 9b. At the applied protein concentration, 1×10^{-5} M (hexamer), the enzyme is in large excess over the nucleic acid, and thermodynamically rigorous fluorescence titrations show that two DnaB hexamers bind to the fork (see above). The solid line in Figure 9b is a nonlinear least-squares fit to a single exponential function (eq 1), indicating that predominately a single species with a molecular weight of 651 000 ± 30 000 is present in the sample, indicating the formation of the complex of two DnaB hexamers with the fork.

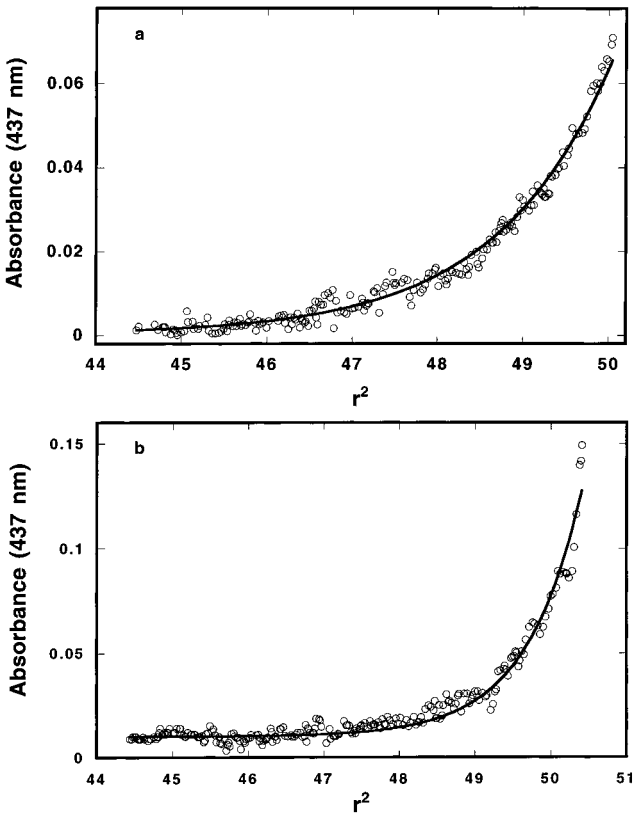

FIGURE 9: (a) Sedimentation equilibrium concentration profile of the 3′ single-arm fork labeled at the 5′ end at the duplex part of the fork with CM in the complex with the DnaB helicase in buffer T2 (pH 8.1, 10 °C) containing 100 mM NaCl and 1 mM AMP-PNP. The duplex part of the fork contains 20 bp (Figure 2a). The protein and nucleic acid concentrations are 1×10^{-5} M (hexamer) and 1×10^{-6} M (fork), respectively. The solid line is a nonlinear least-squares fit to eq 1, with a single sedimenting species having a molecular weight of 355 000 ± 30 000; 6 000 rpm. (b) Sedimentation equilibrium concentration profile of the complex of the two-arm fork labeled at the 5′ end at the duplex part with CM with the DnaB helicase in buffer T2 (pH 8.1, 10 °C) containing 100 mM NaCl and 1 mM AMP-PNP. The duplex part of the fork contains 20 bp (Figure 2a). The protein and nucleic acid concentrations are 1×10^{-5} M (hexamer) and 1×10^{-6} M (fork), respectively. The solid line is a nonlinear least-squares fit to eq 1, with a single sedimenting species having a molecular weight of 651 000 ± 30 000; 6 000 rpm.

Direct Determination of the Orientation of the E. coli DnaB Helicase Bound to the 5′ Arm of a Replication Fork Using the Fluorescence Energy Transfer Method. Determination of the mutual orientations of proteins and nucleic acids in the complex should be based on a method sensitive to the differences in distances between different, specific regions of both macromolecules (*21*, *26*). Fluorescence energy transfer between a donor and an acceptor, placed in specific locations on a protein and a nucleic acid, provides a very sensitive technique to assess the relative proximity between different regions of both macromolecules in the complex. The orientation of the DnaB helicase in the complex with the 5′ arm of the replication fork was determined using a 5′ single-arm fork substrate labeled with fluorescein (acceptor) at the 5′ or 3′ end of the 30 mer constituting the 5′ arm of the substrate as depicted in Figure 10. The DnaB protein monomer is built of two structural domains, a small 12-kDa and a large 33-kDa domain, connected at the "hinge" region (*15*, *16*, *30*). Because the

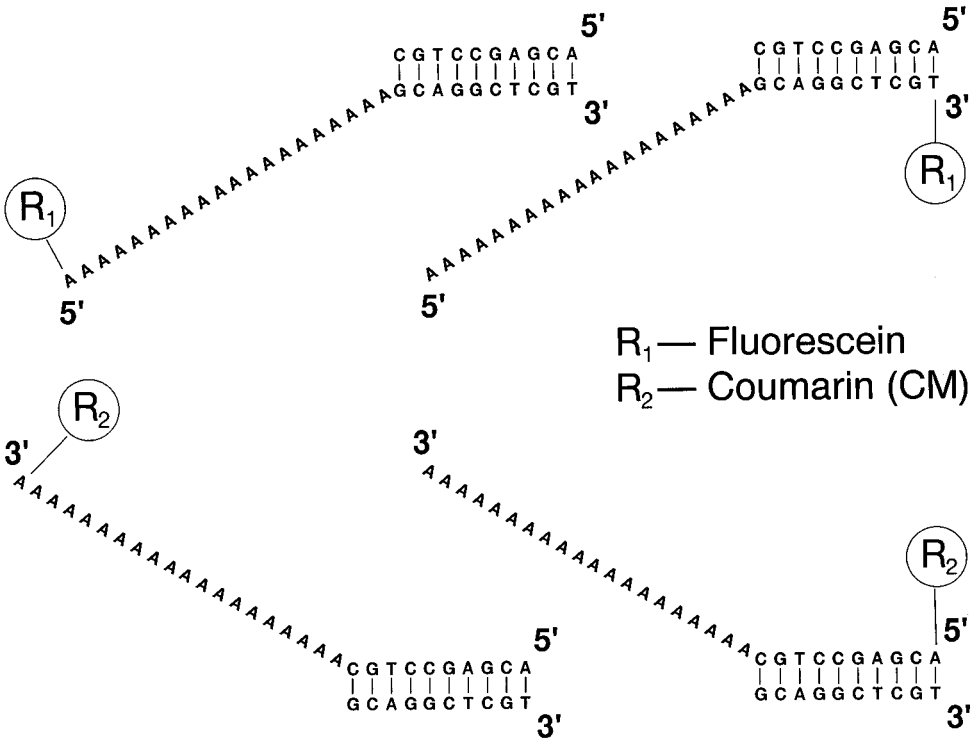

FIGURE 10: Single-arm fork substrates used in the studies of the orientation of the DnaB hexamer in the complexes with the 5′ and 3′ arms of the replication fork. All substrates have a 20 nucleotide long arm built of adenosine residues and a 10 bp long duplex part. The 5′ single-arm fork substrates have a fluorescein residue (R_1) placed at the 5′ end of the arm or at the 3′ end of the duplex part of the fork located on the 30 mer, which constitutes the arm extension of the fork. The 3′ single-arm fork has CM (R_2) placed at the 3′ end of the arm or at the duplex part of the fork located on the 30 mer constituting the arm extension of the fork.

protein does not have natural cysteines, we replaced arginine with a single cysteine residue using site-directed mutagenesis and thus obtained the DnaB protein variant R14C. The selection of the modification site was directed by the fact that removal of the entire 14 amino acid fragment from the N terminus of the protein does not affect to any extent the biological functions of the protein (*30*). The introduced cysteine residues were specifically modified with a fluorescent coumarin derivative (CPM) (see Materials and Methods). As a result of modification, the R14C hexamer has ~6 CPM molecules located in the small domain of each protomer (R14C−CPM). If the DnaB hexamer binds predominantly in a single orientation to the 5′ arm of the fork, then different responses of the donor and acceptor fluorescence should be observed depending on the different location of the acceptor on the nucleic acid.

The corrected emission spectrum of R14C−CPM (λ_{ex} = 435 nm) and the absorption spectrum of the 5′ single-arm fork labeled at the 5′ end of the arm with fluorescein in buffer T2 (pH 8.1, 100 mM NaCl, 1 mM AMP-PNP, 10 °C) are shown in Figure 11a. There is a strong overlap between the emission spectrum of R14C−CPM and the absorption spectrum of the fluorescein-labeled nucleic acid. These spectroscopic properties of CPM make the marker an excellent fluorescence donor for fluorescein (*31*). Fluorescence emission spectra of R14C−CPM (λ_{ex} = 435 nm) in the absence and presence of unlabeled 5′ single-arm fork and the fluorescence emission spectrum of the 5′ single-arm fork labeled at its 5′ end with fluorescein (λ_{ex} = 485 nm) in the absence and presence of R14C−CPM are shown in Figure 11. The presence of an unlabeled fork substrate has very little effect on the CPM fluorescence intensity. However, the presence of R14C−CPM causes an ~31% decrease of the fluorescence intensity of the labeled 5′ single-arm fork, although at 485 nm only fluorescein on the 5′ end of the fork substrate absorbs light. Saturation of the 5′ single-arm fork substrate labeled at the 5′ end with fluorescein with the unlabeled DnaB protein causes only an ~7% decrease of the emission intensity of the fluorescein residue (data not shown). Clearly, the presence of six hydrophobic CPM residues significantly affects the quantum yield of fluorescein at the 5′ end of the DNA substrate, even in the absence of the energy transfer process. The quantum yield of fluorescein is independent of the excitation wavelength between 400 and 500 nm (*26*). Thus, as expected, the ratio of quantum yields of the labeled 5′ single-arm fork in the complex with R14C−CPM and free in solution, (ϕ_B^A/ϕ_F^A), is constant and equals 0.69 over a tested range of excitation wavelengths between 465 and 500 nm. In this spectral range of excitation, no detectable fluorescence energy transfer from CPM residues to fluorescein occurs. Thus, this ratio reflects the decrease of the emission intensity of the 5′ single-arm fork labeled with fluorescein at the 5′ end of the arm in the complex with R14C−CPM, in the absence of the energy transfer process. The value of ϕ_B^A/ϕ_F^A can then be used to obtain the spectrum of the labeled 5′ single-arm fork substrate in the complex with R14C−CPM without the changes induced by the energy transfer process at any excitation wavelength.

The dashed line in Figure 12a is the sum of the emission spectra (λ_{ex} = 435 nm) of R14C−CPM and the 5′ single-arm fork labeled at the 5′ end of the arm with fluorescein in the presence of unlabeled nucleic acid and R14C−CPM (without energy transfer), respectively. The solid line in

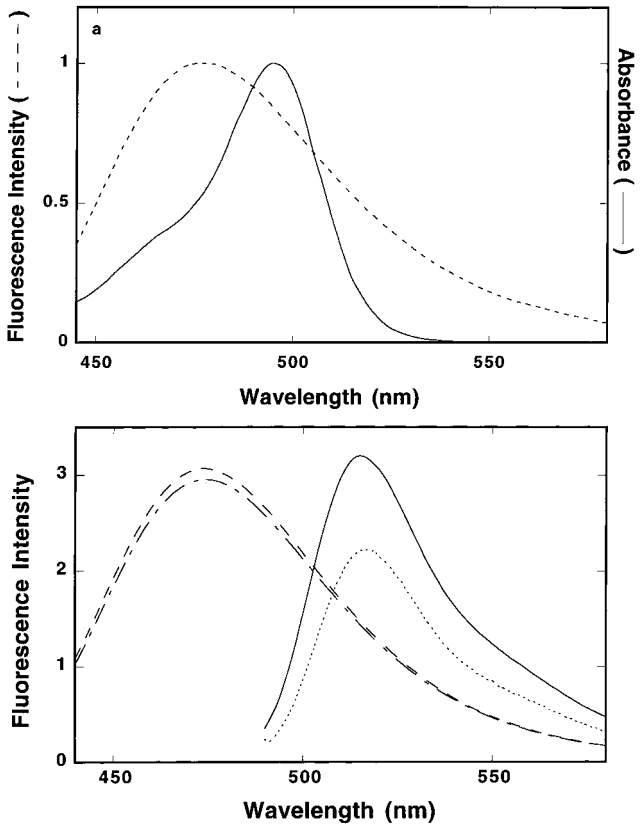

FIGURE 11: (a) Overlap of the fluorescence emission spectrum of the DnaB variant, R14C−CPM (- - -), (λ_{ex} = 435 nm) with the absorption spectrum of the 5′ single-arm fork, labeled at the 5′ end of the arm with fluorescein (Figure 10) in buffer T2 (pH 8.1, 10 °C) containing 100 mM NaCl and 1 mM AMP-PNP (—). (b) Fluorescence emission spectrum of the DnaB variant R14C−CPM in the absence (— —) and presence (— - —) of the unlabeled 5′ single-arm fork (λ_{ex} = 435 nm) in buffer T2 (pH 8.1, 10 °C) containing 100 mM NaCl and 1 mM AMP-PNP. Concentrations of R14C−CPM and the oligomer are 9.6×10^{-7} M (hexamer) and 4.5×10^{-7} M (oligomer), respectively. Fluorescence emission spectrum of a 5′ single-arm fork labeled at the 5′ end of the arm with fluorescein (λ_{ex} = 485 nm) in the absence (—) and presence (• • •) of R14C−CPM (without energy transfer) in buffer T2 (pH 8.1, 10 °C) containing 100 mM NaCl and 1 mM AMP-PNP. Concentrations of the labeled 5′ single-arm fork and the protein are 4.5×10^{-7} M (oligomer) and 9.6×10^{-7} M (hexamer), respectively.

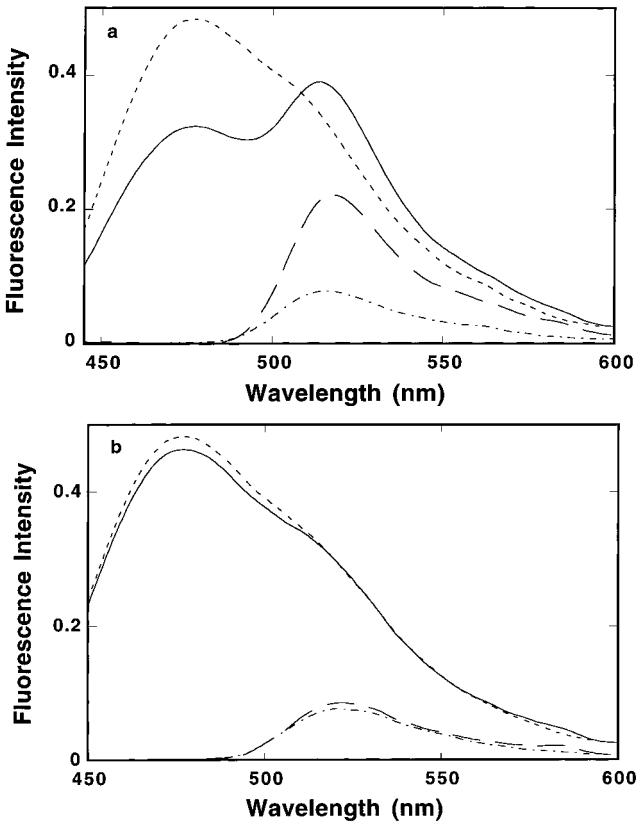

FIGURE 12: (a) Sum of the fluorescence emission spectra of R14C−CPM in the presence of an unlabeled 5′ single-arm fork (4.5×10^{-7} M (fork) and of the 5′ single-arm fork labeled at the 5′ end with fluorescein in the presence of R14C−CPM (without energy transfer) (λ_{ex} = 435 nm) (- - -) in buffer T2 (pH 8.1, 10 °C) containing 100 mM NaCl and 1 mM AMP-PNP. Concentration of R14C−CPM is 9.6×10^{-7} M (hexamer). The fluorescence emission spectrum of the complex of R14C−CPM with a 5′ single-arm fork labeled at the 5′ end with fluorescein (λ_{ex} = 435 nm) (—) in the same buffer. Concentrations of the nucleic acid and the protein are 4.5×10^{-7} M (fork) and 9.6×10^{-7} M (hexamer), respectively. Sensitized emission spectrum of a 5′ single-arm fork labeled at the 5′ end with fluorescein (λ_{ex} = 435 nm) in the complex with R14C−CPM (— —) obtained after subtraction of the normalized spectrum of R14C−CPM superimposed on the fluorescence emission spectrum of the labeled nucleic acid in the presence of R14C−CPM (without energy transfer) (— • —). (b) Sum of the fluorescence emission spectra of R14C−CPM in the presence of the unlabeled 5′ single-arm fork and of the 5′ single-arm fork labeled at the 3′ end of the duplex part of the fork with fluorescein (Figure 10) in the presence of unlabeled DnaB (λ_{ex} = 435 nm) (- - -) in buffer T2 (pH 8.1, 10 °C) containing 100 mM NaCl and 1 mM AMP-PNP. Concentrations of R14C−CPM and the fork are 9.6×10^{-7} M (hexamer) and 4.5×10^{-7} M (fork), respectively. The fluorescence emission spectrum of the complex of R14C−CPM with the 5′ single-arm fork labeled at the 3′ end of the duplex part of the fork with fluorescein (λ_{ex} = 435 nm) in the same solution conditions (—). Concentrations of the nucleic acid and R14C−CPM are 4.5×10^{-7} M (fork) and 9.6×10^{-7} M (hexamer), respectively. Sensitized emission spectrum of the 5′ single-arm fork labeled at the 3′ end of the duplex part of the fork with fluorescein (λ_{ex} = 435 nm) in the complex with R14C−CPM (— —) obtained after subtraction of the normalized spectrum of R14C−CPM and superimposed on the fluorescence emission spectrum of the nucleic acid in the presence of the unlabeled DnaB protein (— • —), obtained at the same excitation wavelength.

Figure 12a is the fluorescence emission spectrum of the complex of R14C−CPM with the labeled fork substrate at the same concentrations of both protein and nucleic acid, as in the case of the independent components of the complex. There is a significant difference between the sum of the independent donor and acceptor spectra and the spectrum where both donor and acceptor are placed in the same complex. The emission intensity at the R14C−CPM maximum at 476 nm in the complex with the labeled 5′ single-arm fork is decreased by ∼33%, as compared to the R14C−CPM complexed with the unlabeled 5′ single-arm fork. The decrease of emission at 476 nm, where there is no contribution from fluorescein emission, indicates strong fluorescence energy transfer from the CPM residues located on the small 12-kDa domains of the DnaB helicase to the fluorescein moiety located at the 5′ end of the arm of the 5′ single-arm fork.

Comparison between the sum of the spectra of independent components of the complex and the spectrum of the complex in Figure 12a shows that the fluorescence intensity of the fluorescein residue of the labeled 5′ single-arm fork, with the peak at ∼520 nm, is strongly increased in the complex with R14C−CPM. Because fluorescein does not contribute to the emission at 476 nm, we can normalize the spectrum

of R14C−CPM in the complex with the unlabeled 5′ single-arm fork to the spectrum of the complex of R14C−CPM with the labeled 5′ single-arm fork at 476 nm. The difference between the normalized spectrum of the complex of R14C−CPM with the unlabeled 5′ single-arm fork and the spectrum of the complex of R14C−CPM with the labeled 5′ single-arm fork provides the sensitized emission spectrum of the labeled 5′ single-arm fork in the complex with R14C−CPM. The emission spectrum of the 5′ single-arm fork labeled at the end of the 5′ arm with fluorescein in the complex with R14C−CPM without energy transfer and the sensitized emission spectrum of the labeled fork in the complex with R14C−CPM are included in Figure 12a. It is evident that, in the presence of the donor (CPM) the fluorescence intensity of fluorescein at the 5′ end of the 5′ arm of the fork is increased by ∼180%.

Subsequently, analogous experiments have been performed with the 5′ single-arm fork with the fluorescein located at the opposite 3′ end of the substrate on the same 30 mer (see Figure 10). Unlike the case of the 5′ single-arm fork, labeled at the 5′ end of the arm with fluorescein, the formation of the complex with R14C−CPM causes only an ∼10% decrease of the emission intensity of the fork substrate labeled at the 3′ end at the duplex part of the fork (data not shown). The effect is the same as that observed in the complex of this labeled fork substrate with the unlabeled DnaB protein. The dashed line in Figure 12b is the sum of the fluorescence emission spectra of R14C−CPM and the fluorescence emission spectrum of the 3′ single-arm fork labeled with fluorescein at the 3′ end at the duplex part of the fork in the presence of the unlabeled 3′ single-arm fork and the unlabeled DnaB protein, respectively, in buffer T2 (pH 8.1, 10 °C) containing 100 mM NaCl and 1 mM AMP-PNP (λ_{ex} = 435 nm). The solid line in Figure 12b is the fluorescence emission spectrum of the complex of R14C−CPM with the 5′ single-arm fork labeled with fluorescein at the 3′ end of the duplex part of the fork at the same concentrations of the protein and nucleic acid as independent components of the complex. Contrary to the situation when the fluorescein is located at the 5′ end of the arm of the fork, there is only an ∼5% decrease of the CPM fluorescence when both the donor (CPM on the DnaB protein) and the acceptor (fluorescein on the 3′ end of the duplex part of fork) are placed in the same complex as compared to the sum of the spectra of independent components of the complex. Also, the sensitized emission spectrum of the fluorescein located at the 3′ end of the duplex part the fork substrate is only increased by ∼12% over the spectrum of the fork substrate in the absence of the donor. These spectral properties indicate a very diminished fluorescence energy transfer from CPM to the fluorescein moiety when the fluorescein is located at the 3′ end of the duplex part of the fork substrate.

The dramatic difference between the emission spectrum of the R14C−CPM complex with the single-arm fork labeled at the 5′ end of the arm and the spectrum of the complex with the single-arm fork labeled at the 3′ end in the duplex part of the fork clearly shows that the helicase binds to the 5′ arm of the fork in a single orientation, with small 12-kDa domains of protomers of the hexamer facing the 5′ end of the arm. This result is in excellent agreement with our recent fluorescence energy transfer studies, which showed that the enzyme binds ssDNA in one orientation with the 5′ end of the nucleic acid in close proximity to the 12-kDa domains of the hexamer (Jezewska et al., manuscript in preparation). The effect of the location of the fluorescence acceptor on the observed spectra properties of the studied complexes is reflected in the large differences in the Förster energy transfer efficiencies (E). Using eqs 5b and 7, we obtained the apparent transfer efficiencies of $E_D = 0.73 \pm 0.03$ and $E_A = 0.50 \pm 0.03$, respectively, for the R14C−CPM complex with the 5′ single-arm fork labeled with fluorescein at 5′ end of the arm. This difference between E_D and E_A indicates that fluorescein at the 5′ end of the bound 5′ single-arm fork induces additional nondipolar quenching of the CPM fluorescence. The true Förster fluorescence transfer efficiency from CPM located on the small 12-kDa domain to the fluorescein residue at the 5′ end of the arm of the fork substrate is then described by eq 8, which provides $E = 0.65 \pm 0.03$. This value of E indicates that the distance between the center of the mass of CPM residues on the DnaB hexamer and fluorescein at the 5′ end is shorter than the Förster critical distance (R_o) for this donor−acceptor pair (eq 9). In the case of the 5′ single-arm fork, where fluorescein is located at the 3′ end in the duplex part of the fork, $E_D = E_A = E = 0.04 \pm 0.01$ indicates that the distance from the center of mass of the donors (CPM) and the acceptor (fluorescein) is ∼2-fold longer than the Förster distance (R_o) (eq 9; see Discussion).

Direct Determination of the Orientation of the E. coli DnaB Helicase Bound to the 3′ Arm of a Replication Fork. Thermodynamic and fluorescence studies of the DnaB helicase interactions with replication fork substrates (described above) indicate that the enzyme is bound in an opposite orientation with respect to the duplex part of the fork in the complex with the 3′ arm, as compared to the complex with the 5′ arm. Because, in the complex with the 5′ single-arm fork, the 12-kDa domains of the DnaB protomers face the 5′ end of the arm (see above), binding of the hexamer in an opposite orientation in the complex with the 3′ arm of the fork will place 12-kDa domains in closer proximity to the 5′ end of the 10 bp long duplex part of the fork than the 3′ end of the 20 nucleotide residues long 3′ arm (Figure 10). This difference in proximities should be reflected in the significant difference in the fluorescence energy transfer efficiencies between a donor and an acceptor located at the 3′ and 5′ ends of the nucleic acid and the small domains of the DnaB hexamer. The direct examination of the orientation of the DnaB hexamer, when bound to the 3′ arm of the fork substrate, has been determined using the DnaB variant R14C labeled at the 12-kDa domain with fluorescein (R14C−Fl). As a DNA substrate, we used the 3′ single-arm fork with the coumarin derivative (CM) at the 3′ end of the arm or at the opposite 5′ end of the 30 mer in the duplex part of the fork as depicted in Figure 10. The emission spectrum of this coumarin derivative overlaps the absorption spectrum of fluorescein to a similar extent as the CPM emission spectrum (data not shown); however, it is spectroscopically different from CPM. It has a maximum of absorption spectrum red-shifted by 45 nm and an absorption coefficient significantly higher than CPM (Materials and Methods).

The dashed line in Figure 13a is the sum of the emission spectra (λ_{ex} = 435 nm) of R14C−Fl and the 3′ single-arm

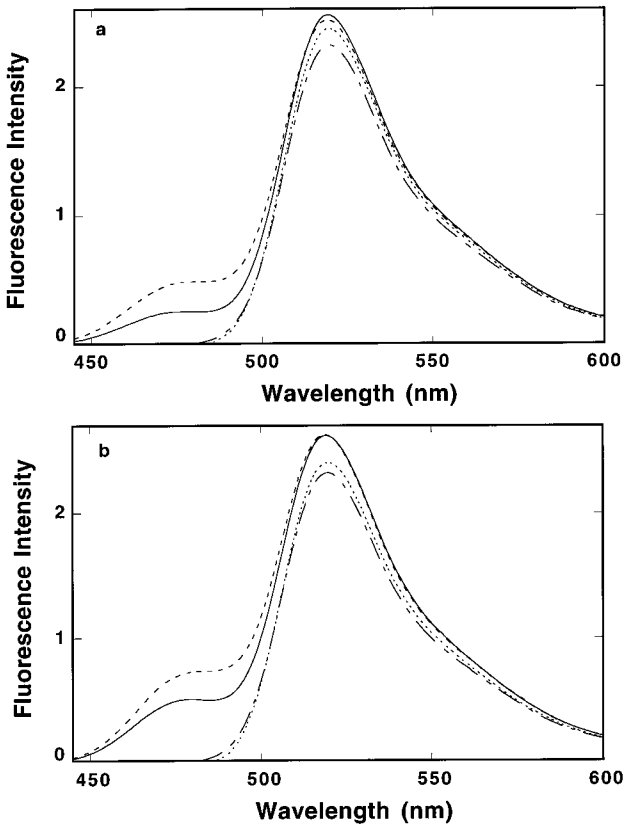

FIGURE 13: (a) Sum of the fluorescence emission spectra of R14C−Fl in the presence of an unlabeled 3′ single-arm fork and of the 3′ single-arm fork labeled at the 3′ end of the arm with CM, in the presence of the unlabeled DnaB protein, respectively (λ_{ex} = 435 nm) (- - -) in buffer T2 (pH 8.1, 10 °C) containing 100 mM NaCl and 1 mM AMP-PNP. Fluorescence emission spectrum of the complex of R14C−Fl with a 3′ single-arm fork labeled at the 3′ end of the arm with CM (λ_{ex} = 435 nm) (—) in the same buffer. Concentrations of the nucleic acid and the protein are 4.5×10^{-7} M (fork) and 9.6×10^{-7} M (hexamer), respectively. Sensitized emission spectrum of R14C−Fl (•••) in the complex with the 3′ single-arm fork labeled at the 3′ end of the arm with CM (λ_{ex} = 435 nm) obtained after subtraction of the normalized spectrum of the labeled nucleic acid and superimposed on the fluorescence emission spectrum of R14C−Fl in the presence of the unlabeled 3′ single-arm fork (without energy transfer) (— - —) obtained at the same excitation wavelength. (b) Sum of the fluorescence emission spectrum of R14C−Fl in the presence of an unlabeled 3′ single-arm fork and fluorescence emission spectrum of a 3′ single-arm fork, labeled at the 5′ end of the duplex part of the fork with CM in the presence of an unlabeled DnaB protein (λ_{ex} = 435 nm) in buffer T2 (pH 8.1, 10 °C) containing 100 mM NaCl and 1 mM AMP-PNP (— —). Concentrations of the fork substrate and the protein are 4.5×10^{-7} M (fork) and 9.6×10^{-7} M (hexamer), respectively. Fluorescence emission spectrum of the complex of R14C−Fl with the 3′ single-arm fork labeled at the 5′ end of the duplex part of the fork with CM (λ_{ex} = 435 nm) in the same solution conditions (—). Concentrations of the labeled nucleic acid and the labeled protein are 4.5×10^{-7} M (fork) and 9.6×10^{-7} M (hexamer), respectively. Sensitized emission spectrum of the 3′ single-arm fork labeled at the 5′ end of the duplex part of the fork with CM (λ_{ex} = 435 nm) in the complex with R14C−Fl (•••) obtained after subtraction of the normalized spectrum of the 3′ single-arm fork labeled at the 5′ end of the duplex part of the fork with CM and superimposed on the emission spectrum of the nucleic acid in the presence of an unlabeled DnaB protein (— - —).

fork labeled at the 5′ end of the duplex part of the fork with CM (Figure 10) in the presence of the unlabeled 3′ single-arm fork and the unlabeled protein, respectively. The solid line is the fluorescence emission spectrum of the complex of R14C−Fl and the labeled nucleic acid at the same concentrations of the protein and fork, as in the case of the independent components of the complex. The difference between the sum of the independent donor and acceptor spectra and the spectrum where both donor and acceptor are placed in the same complex is significant. The emission intensity at the maximum (478 nm) of the 3′ single-arm fork labeled with CM at the 5′ end of the duplex part of the fork in the complex with R14C−Fl is decreased by ∼43% as compared to the labeled 3′ single-arm fork complexed with unlabeled DnaB protein. As in the case of CPM discussed above, the decrease of the donor emission indicates significant fluorescence energy transfer from the CM residue located at the 5′ end of the duplex part of the 3′ single-arm fork to the fluorescein moiety located on the small 12-kDa domains of the DnaB hexamer.

Comparison between the sum of the spectra of independent components and the spectrum of the complex in Figure 13a shows that the fluorescence intensity of R14C−Fl is increased in the complex with the 3′ single-arm fork labeled at the 5′ end of the duplex part of the arm. As in the case of the 5′ single-arm fork in the complex with R14C−CPM discussed above, fluorescein does not contribute to the CM emission band at the maximum (478 nm); thus, we can normalize the spectra of the nucleic acid to its spectrum in the complex with R14C−Fl at 478 nm. Subtracting the normalized spectrum from the spectrum of the complex provides the sensitized emission spectrum of R14C−Fl in the complex with the 3′ single-arm fork labeled at the 5′ end of the duplex part. The sensitized emission spectrum of R14C−Fl and the emission spectrum of R14C−Fl in the complex with the unlabeled 3′ single-arm fork, where no energy transfer occurs, are shown in Figure 13a.

Next, we examined the fluorescence energy transfer process from CM located at the 3′ end of the arm of the 3′ single-arm fork substrate (Figure 10) to fluorescein residues on R14C−Fl. The dashed line in Figure 13b is the sum of the fluorescence emission spectrum of R14C−Fl and the fluorescence emission spectrum of the 3′ single-arm fork labeled at the 3′ end of the arm of the fork with CM in the presence of the unlabeled 3′-single-arm fork and the unlabeled DnaB protein, respectively, in buffer T2 (pH 8.1, 10 ° C) containing 100 mM NaCl and 1 mM AMP-PNP (λ_{ex} = 435 nm). The solid line in Figure 13b is the fluorescence emission spectrum of the complex of R14C−Fl with the 3′ single-arm fork labeled at the 3′ end of the arm with CM at the same concentrations of the protein and nucleic acid as independent components of the complex. The emission intensity at the nucleic acid, maximum at 478 nm, in the complex with R14C−Fl is decreased by ∼30%, which is a significantly lower quenching when compared to the complex of R14C−Fl with the 3′ single-arm fork labeled at the 5′ end of the duplex part of the fork. This smaller decrease of emission indicates less efficient fluorescence energy transfer from the CM residue located at the 3′ end of the arm of the fork to fluorescein placed on the small 12-kDa domain of the DnaB hexamer. Also, the sensitized emission spectrum of R14C−Fl in the complex with the 3′ single-arm fork labeled at the 3′ end of the arm of the fork is lower when compared to the corresponding sensitized emission of R14C−Fl in the complex with the fork substrate labeled at the 5′ end of the duplex part of the fork (see Figure 13a).

Using eqs 5b and 7, we obtained the apparent transfer efficiencies of $E_D = 0.7 \pm 0.05$ and $E_A = 0.18 \pm 0.02$, respectively, for the R14C−CPM complex with the 3′ single-arm fork labeled at the 5′ end of the duplex part of the fork with CM. The Förster transfer efficiency from CM at the 5′ end of the duplex part of the 3′ single-arm fork and fluorescein located on the small 12-kDa domains is then $E = 0.38 \pm 0.03$ (eq 8). In the case of the single-arm fork, where CM is located at the opposite 3′ end of the arm of the fork substrate, $E_D = 0.44 \pm 0.03$ and $E_A = 0.14 \pm 0.02$, respectively, thus providing $E = 0.2 \pm 0.02$. This large difference between the values of E indicates significantly closer proximity of the donor (CM) at the 5′ end of the duplex part of the 3′ single-arm fork and the center of mass of acceptors on the 12-kDa domains of the DnaB hexamer as compared to the R14C−Fl complex with the fork substrate labeled at the 3′ end of the arm. These data directly show that the helicase forms a complex with the 3′ arm of the fork in which small 12-kDa domains of protomers of the hexamer face the duplex part of the arm. Thus, the DnaB hexamer binds the 3′ arm of the replication fork in the reverse orientation as compared to the DnaB hexamer associated with the 5′ arm of the fork. Notice that the binding of the helicase in opposite orientations to the 5′ and 3′ arms of the replication fork means that the enzyme always binds with the same orientation with respect to the polarity of the sugar−phosphate backbone of the ssDNA, which is reverse in both arms of the fork. In other words, the enzyme binds ssDNA in strictly one orientation in which the 5′ end of the nucleic acid is in close proximity to the 12-kDa domains of the hexamer and the 3′ end of the ss nucleic acid is at the large 33-kDa domain of the protein (Jezewska et al., manuscript in preparation, see Discussion).

DISCUSSION

Elucidation of the interactions of the replicative helicase with the replication fork is of paramount importance for our understanding of the mechanism of the enzyme. Still, little is known about these interactions. In this work, we described intensive thermodynamic and structural studies of the *E. coli* primary replicative helicase DnaB protein with various replication fork substrates. We utilized the fact that interactions of the DnaB protein with ethenoadenosine (ϵA) are accompanied by a large nucleic acid fluorescence increase (*10*−*12*, *17*, *18*). The ethenoadenosine phosphates are characterized by strong blue fluorescence with the maximum around 400 nm and the quantum yield ∼0.55 (*20*, *22*, *32*). Although the emission of ϵA depends little upon the environment, placing of ϵA in a polymer nucleic acid diminishes its fluorescence by ∼10−12-fold due to complex quenching interactions with adjacent bases (*32*, *33*). A strong increase of the ϵA fluorescence of a nucleic acid substrate in the complex with a protein with excitation far from the protein absorption band indicates a conformational change of the nucleic acid, most probably significant separation and immobilization of the bases interacting with the binding site that eliminates part of the quenching processes.

The replication fork substrates used in this work contain a stretch of six ϵAs in the arms of the forks (Figure 2a,b). Because we are interested in the intrinsic affinity of the enzyme for the arms, the length of the arms has been selected to exactly correspond to the site size of the DnaB hexamer−ssDNA complex, i.e., 20 nucleotide residues. Therefore, each arm can accommodate only a single DnaB helicase, and the binding should reflect the intrinsic affinity without major statistical factor corrections[2] (*17*).

Role of dsDNA in Preferential Binding of the DnaB Helicase to the 5′ Arm of a Replication Fork. Quantitative analysis of DnaB interactions with single-arm fork substrates shows that, in the presence of the ATP nonhydrolyzable analogue (AMP-PNP), the helicase binds with a higher affinity to the 5′ arm than to the 3′ arm of the fork. This preferential affinity for the 5′ arm is only slightly dependent on the length of the duplex part of the fork substrate (Figure 5; *18*). Moreover, the affinities of the enzyme for the 5′ single-arm fork and the 20 mer, $dA(pA)_6(p\epsilon A)_6(pA)_7$, corresponding to the isolated arm are within experimental accuracy the same, indicating that the duplex part of the fork provides no contribution to the free energy of binding of the helicase (*18*). Analytical ultracentrifugation experiments also show that, independent of the protein concentrations, only a single hexamer can bind to single-arm fork substrates. Because the helicase binds ssDNA without preference for the ends of the nucleic acid, the data suggest that, in the complex with the fork, the helicase accommodates the duplex part of the fork in the active site without additional free energy changes and that the binding free energy predominantly originates from interactions with the ssDNA of the arm. On the other hand, the maximum fluorescence increase in the interactions of the enzyme with the 5′ arm of the fork substrate, having a 20 bp long duplex part ($\Delta F_{max} = 1.7$) is much lower than the $\Delta F_{max} = 2.7$ observed for the complex with the 3′ single-arm fork. This is in contrast to approximately the same $\Delta F_{max} = 1.2$ observed for the fork substrates with only a 10 bp long dsDNA (Figure 5; *18*). These results indicate that, while the duplex part of the fork is not contributing to the free energy of binding, it is affecting the way the enzyme induces the conformational changes in the complex with the 5′ or 3′ arm. In the absence of the duplex part of the fork, both the 5′ and 3′ arms of our single-arm fork substrates are physically indistinguishable (Figure 2a). If the duplex part of the fork was not affecting the orientation of the helicase in the fork, the binding of the helicase to the 3′ single-arm fork would be characterized by the same fluorescence changes and the same affinity as in the case of the 5′ single-arm fork or the isolated 20 mer, which is not experimentally observed.

[2] In our previous works (*10*, *17*), we determined that the cooperativity in the binding of the DnaB helicase to 40 mer, which can only accommodate two DnaB hexamers, is characterized by a value of cooperativity parameter $\omega = 0.03$, which is much lower than $\omega \sim 5$ determined for the binding to the polymer ssDNA. This low estimate, which suggested significant end effects in the binding of the helicase to ssDNA oligomers, was due to an error in the computer program. The correct value of the cooperativity parameter for the binding of the DnaB helicase to 40 mer is 10 ± 5 which is very similar to the value determined for polymer ssDNA and indicates the lack of any end effect in the helicase binding. In additional studies, we performed binding studies with different 40 mers having stretches of 10 ϵAs at the 5′ end, in the middle, and at the 3′ end of the oligomer. A preferential binding to the 5′ or 3′ end means that the ends act as distinct binding sites within the context of the rest of the nucleic acid. If the helicase binds preferentially to the ends of the nucleic acid, significant differences in the measured affinities between different oligomers labeled at the ends and in the middle should be observed. No significant differences have been observed, thus showing the lack of an end effect in the binding of the DnaB helicase to ssDNA.

The lower affinity of the helicase for the 3′ single-arm fork and the different fluorescence changes of the ϵA in the arm also indicate that the enzyme is oriented differently as compared to its orientation in the complex with 5′ single-arm fork, resulting in the different effect of the duplex part of the fork on the interactions of the enzyme with the arm.

In the Complex with the 5′ Arm of the Fork the DnaB Helicase Binds in a Strict Orientation with the Large 33-kDa Domain Facing the Duplex Part of the Fork. As we pointed out, the determination of the mutual orientation of the protein and nucleic acid in a complex should be based on the method that is sensitive to the differences in distances between different specific regions of both macromolecules. The fluorescence energy transfer technique is such a method. The difference in the effect of the location of the acceptor (fluorescein) at the 5′ end of the arm and the 3′ end of the dsDNA on the fluorescence spectra of the complex of nucleic acid with R14C−CPM (excited in a predominantly donor absorption band) is dramatic. While in the complex with the 5′ single-arm fork labeled at the 5′ end of the arm, the fluorescence of R14C−CPM is quenched by ∼33% and the emission of fluorescein is increased by ∼180%, only an ∼5% decrease of the CPM fluorescence and an ∼12% increase of the emission intensity of fluorescein, respectively, are observed in the complex of R14C−CPM when fluorescein is located at the 3′ end of the duplex part of the fork (Figure 12a,b). These dramatic spectral differences are reflected in the large differences between the energy transfer efficiencies from CPM in the small domains, all located at one end of the DnaB hexamer, and the fluorescein located at the 5′ or 3′ end of the fork substrate. The fluorescence transfer efficiency (E) for the fluorescein placed at the 5′ end of the arm is 0.65 ± 0.03. The transfer efficiency for the same acceptor located at the 3′ end of the duplex part of the fork is only 0.04 ± 0.01. In the case of chemically identical donor−acceptor pairs, the transfer efficiency depends on two variable factors characteristic for the studied system, the distance between the donor and acceptor (R) and the orientation parameter (κ^2) which characterizes the mutual orientation of the donor absorption dipole and acceptor emission dipole (*26*). The value of κ^2 can theoretically assume any value between 0 and 4, but only these two extreme values would significantly affect the determined transfer efficiency. The possible range of κ^2 can be estimated by using the standard procedure (*29*). The determined limiting anisotropies of R14C−CPM and fluorescein located at the 5′ end of the arm and at the 3′ end of the duplex part of the 5′ single-arm fork in the complex with the enzyme are 0.25 ± 0.01, 0.29 ± 0.01, and 0.21 ± 0.01, respectively. These values provide the ranges of $0.12 < \kappa^2 < 3.1$ and $0.21 < \kappa^2 < 2.8$, thus very similar for both fork substrates labeled with fluorescein at opposite ends and away from the extreme values of 0 and 4 (*29*). Another equally rigorous procedure (but more time-consuming and more expensive) that provides the information on the effect of κ^2 on measured transfer efficiency is to perform experiments with several different donor−acceptor pairs, which due to different structures of different chromophores provide the necessary "randomization" of the orientations of emission and absorption dipoles (*34*). Using several different donor−acceptor pairs placed in the small domain of the protein and at the 5′ and 3′ ends of the nucleic acid, we obtained a similar, very large difference between the fluorescence transfer efficiencies for donors and acceptors located on the small 12-kDa domains and on the opposite ends of the fork substrates (data not shown). The results clearly show that the large difference between the transfer efficiencies results from the large difference in the distances between the opposite ends of the 5′ single-arm fork substrate and the CPM located on the small domain of the DnaB protomers. The determination of exact distances between the donors (CPM) and acceptors (fluorescein) is beyond the scope of the present discussion on the orientation of the DnaB helicase in the complex with the replication fork. However, using eq 10, we can estimate the approximate ratio of the distances between the 5′ and 3′ ends of the fork substrate from the center of the mass of CPM donors located on the small domains of the DnaB hexamer. Introducing $E_1 = 0.65$ and $E_2 = 0.04$ into eq 10, we obtain $R_1/R_2 = 0.53$. Thus, the distance of the 5′ end of the arm of the fork is approximately two times shorter than the distance between the donors in the small domains and the 3′ end of the duplex part of the fork.

Our data show that the DnaB helicase binds the 5′ arm of the replication fork in a single orientation. In the complex with the arm, the small domain of the protein is in close proximity to the 5′ end of the arm, while the large domain is facing the duplex part of the fork. Recently, we obtained direct evidence that the DnaB helicase binds ssDNA in a strict, single orientation with respect to the sugar−phosphate backbone of the nucleic acid (Jezewska et al., manuscript in preparation). In the complex with ssDNA, the enzyme binds with small domains adjacent to the 5′ end of the nucleic acid, while the large 33-kDa domains are close to the 3′ end. Thus strict orientation of the helicase in the complex with the 5′ arm of the fork reflects the single orientation in the binding of the enzyme with respect to the polarity of the ssDNA of the arm.

In the Complex with the 3′ Arm of the Fork the DnaB Helicase Binds in an Opposite Orientation with Respect to the Duplex Part of the Fork Than in the Complex with the 5′ Arm. Quantitative fluorescence titrations discussed above indicate that the orientation of the DnaB helicase in the complex with the 3′ arm of the fork is opposite to the orientation of the enzyme in the complex with the 5′ arm. Fluorescence energy transfer experiments provide direct evidence that this is the case. The 3′ single-arm fork substrates used in these experiments are depicted in Figure 10. If the helicase binds to the 3′ arm in the same orientation as to the 5′ arm, then the 12-kDa domains labeled with fluorescein would be in close proximity to the 3′ end of the arm and at a large distance from the 5′ end of the duplex part of the fork substrate. As a result, a high energy transfer efficiency from the CM residue at the 3′ end of the arm and the very low energy transfer efficiency from the CM at the 5′ end of the duplex part of the fork substrate to the fluorescein moiety should occur. However, this is not what is experimentally observed. Contrary, the transfer efficiency from the CM at the 3′ end of the arm is only 0.20 ± 0.02 as compared to $E = 0.38 \pm 0.03$ from the CM located at the 5′ end of the duplex part of the 3′ single-arm fork. This can only occur if the large DnaB hexamer associated with the 3′ arm of the fork is bound with small 12-kDa domains facing the duplex part of the fork, thus in an opposite orientation as compared to the complex with the 5′ arm. A model of

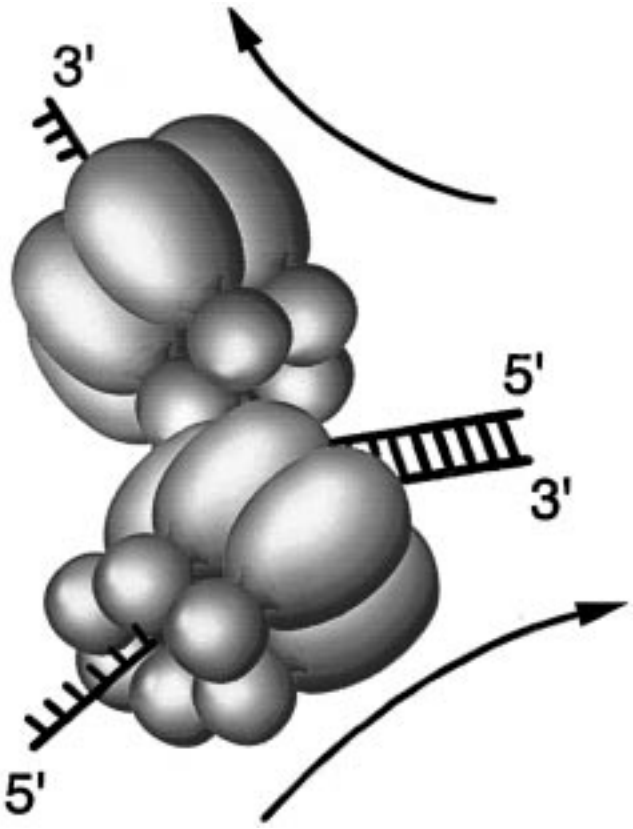

FIGURE 14: Schematic representation of the orientation of two DnaB hexamers bound to the 5′ and 3′ arms of a replication fork, based on results obtained in this work. The hexamer associated with the 5′ arm is facing the duplex part of the fork with the large 33-kDa domains, while the small 12-kDa domains are at the 5′ end of the 5′ arm. The hexamer associated with the 3′ arm is bound in an opposite orientation as compared to the complex with the 5′ arm, thus, with the large 33-kDa domains facing the 3′ end of the arm and the small 12-kDa domains being in close proximity to the duplex DNA. The arrows indicate the 5′ → 3′ direction of the translocation of the enzyme and the unwinding reaction. It is very possible that a similar complex is formed at oriC in the initial stages of the bidirectional replication of the chromosomal DNA in *E. coli*.

the DnaB hexamers associated with the 5′ and 3′ arms of the replication fork is shown in Figure 14. Notice that when the DnaB hexamer is bound to the 3′ arm, all small 12-kDa domains labeled with fluorescein are separated from the 3′ end of the arm by a distance of ∼20 nucleotide residues and by a distance of ∼10 bp from the 5′ end of the duplex part of the fork. This differs from the complex of the enzyme with the 5′ arm where the 5′ end of the arm is in very close proximity to the 12-kDa domains, but at a much larger distance of ∼20 nucleotide residues plus a 10 bp long dsDNA from the 3′ end of the duplex part of the fork. This difference is reflected in the values of the ratios of fluorescence energy transfer efficiencies. The energy transfer efficiency from CPM on the 12-kDa domains to fluorescein at the 5′ end of the arm in the complex of the helicase with the 5′ single-arm fork is ∼12 times higher than the transfer efficiency from the CPM to fluorescein at the 3′ end of the duplex part of the 5′ single-arm fork. The same ratio of the transfer efficiencies is only ∼2 in the case of the helicase complex with the labeled 3′ single-arm fork (Figure 13).

As we pointed out, the DnaB helicase binds ssDNA with a strict, single orientation with respect to the sugar−phosphate backbone of the nucleic acid (see above, Jezewska et al., manuscript in preparation). Thus, our data show that the orientation of the helicase bound to the different arms of the fork is decided by the polarity of the ssDNA, which is opposite in the 5′ and 3′ arms of the replication fork. These results provide a simple explanation of the different affinities between the 5′ and 3′ arms. Recall that the DnaB helicase unwinds dsDNA in the 5′ → 3′ direction (*3*). Therefore, only in the complex with the 5′ arm is the active site of the enzyme in contact with dsDNA, providing the accommodation for this conformation of the nucleic acid. In the complex with the 3′ arm, the active site of the helicase faces the 3′ end of the arm. Such binding must introduce steric hindrances not encountered in the case of the complex with the 5′ single-arm fork substrate where the dsDNA can be accommodated in the active site, resulting in the lower affinity of the enzyme for the 3′ single-arm fork as experimentally observed.

The DnaB Helicase Accesses the Entire 5′ or 3′ Arm in the Complex with the Arms. The Heterogeneity of the DNA Binding Site of a Helicase. The experiments with the fork substrates labeled with ϵA in different locations of the 5′ arm show that, independently of the location of ethenoadenosines, the DnaB protein significantly affects the nucleic acid fluorescence (Figure 8), an indication that the enzyme accesses the entire arm of the fork in the complex. However, the extent of the fluorescence increase is different for different substrates with the largest $\Delta F_{max} = 1.7 \pm 0.2$ observed when the ϵAs are in the middle of the arm and the lowest $\Delta F_{max} = 0.5 \pm 0.1$ when the ϵAs are at the duplex part of the fork. As we pointed out, the DNA binding site of a helicase must provide accommodations for both ss and dsDNA. In this capacity, the site is most probably functionally and structurally heterogeneous. The observed differences in the effect of the enzyme on the conformation of the ssDNA bound to the binding site indicate the existence of such heterogeneity. The heterogeneity of the binding site is also evident in the complex of the helicase with the 3′ arm of the fork where the enzyme exerts distinct effects on the conformation of the ssDNA in different regions of the arm, although the fluorescence changes are different as compared to the changes in the complex with the 5′ arm (Figure 8). These differences between the conformation of the 5′ and 3′ arm in the complex with the helicase reflect the different orientations of the enzyme when bound to the 5′ or 3′ arm of the fork.

The 3′ Arm of the Replication Fork Is Not Engaged in Stable Interactions with the Helicase Associated with the 5′ Arm. Comparison between fluorescence titrations of the 5′ single-arm fork and the two-arm fork substrate labeled at both arms with ϵAs shows that the high affinity step in the binding of the DnaB hexamer to the two-arm fork occurs in exactly the same concentration range of the protein as the binding to the 5′ single-arm substrate. Independently of any models of helicase binding to the fork, this result shows that the binding constant of the helicase for the 5′ arm in the two-arm fork is not affected by the presence of the 3′ arm. Also, notice that the presence of the 3′ arm does not affect the positioning of the helicase on the 5′ arm, as reflected by the unaltered fluorescence change of the ϵAs accompanying the binding of the enzyme to the 5′ arm of the two-arm fork substrates labeled on both arms as well as only on the 5′

arm. The lack of the effect of the 3′ arm on the affinity and positioning of the DnaB hexamer associated with the 5′ arm of the fork indicates that the 3′ arm does not form a thermodynamically stable complex with the DnaB hexamer associated with the 5′ arm of the fork. Moreover, quantitative analysis of the simultaneous binding of two DnaB hexamers to two-arm fork substrates performed with the fork substrate having both arms or only the 5′ arm labeled indicates that the intrinsic affinity of the DnaB hexamer to the 3′ arm and the fluorescence change accompanying the binding is unaffected by the presence of another hexamer already associated with the 5′ arm. The association is characterized by the same K_2 and ΔF_{max} as the interactions of the enzyme with the 3′ single-arm fork. These data indicate that, although the 5′ arm of the fork is already occupied by the enzyme, the 3′ arm is in a conformation in which it is easily available for the binding of the next DnaB hexamer. Because of the large size of the DnaB hexamer, the data suggest that the conformation of the 3′ arm of the fork in the complex with the helicase associated with the 5′ arm must be such that the 3′ arm can bind an additional large DnaB hexamer with very similar affinity as in the independent binding to the 3′ single-arm fork. The studies performed here on a stationary complex of the DnaB helicase with replication fork substrates without ATP hydrolysis do not exclude a significant role of the 3′ arm in the unwinding reaction. It has been indicated that the unwinding reaction of dsDNA by the DnaB helicase fueled by ATP hydrolysis requires the presence of a 3′ arm (*3*). The role of the 3′ arm in the unwinding process is still unknown and requires further thermodynamic and kinetic analysis. The data described in this and our previous work (*18*) indicate that the 3′ arm is only transiently required in the unwinding reaction, possibly interacting with one of the conformational states of the enzyme generated during ATP hydrolysis reaction.

Based on EM studies of the *E. coli* RuvB protein and bacteriophage T7 helicase/primase, it has been proposed that in the complex of a hexameric helicase with a ssDNA the DNA molecule goes through the cross channel of the ring-like structure of the protein (*14*, *35*). The structure of the ssDNA−DnaB helicase complex is currently being studied in our laboratory using fluorescence energy transfer methods. These results indicate that, in the case of the DnaB helicase, the ssDNA also passes the inner channel of the hexamer (Jezewska, unpublished data). Our data show that only the 5′ arm of the fork is predominately engaged in the stationary complex with the single DnaB helicase associated with the fork. Notice that the fluorescence energy transfer efficiency from the CPM on the small 12-kDa domains to the fluorescein residue at the 3′ end of the duplex part of the 5′ single -arm fork is only 0.04 ± 0.01. This result indicates that the enzyme, which engages the entire 5′ arm in the complex, does not occlude a significant number of base pairs of the duplex part of the fork in its active site. With the 5′ arm, i.e., the leading strand of the fork, crossing the inner channel of the hexamer, the separation of the 3′ arm from the 5′ arm indicates that the 3′ arm is protruding in front of the enzyme.

Replication of the chromosomal DNA in *E. coli* is a bidirectional process that begins at a specific site (oriC). From oriC, two replication forks move in opposite directions (*2*). Although the exact stoichiometry of the initial replication complex at oriC is still unknown, the fact that two DnaB hexamers can form a complex (such as is depicted in Figure 14) suggests the possibility that a complex of this type may exist at the early stages of bidirectional DNA replication at oriC. As initiation of the DNA replication proceeds, the two DnaB hexamers bound in opposite orientations to each arm of the formed fork could begin the unwinding of a duplex DNA in different directions.

ACKNOWLEDGMENT

We thank Gloria Drennan Davis for her help in preparing the manuscript.

REFERENCES

1. Lohman, T. M., and Bjornson, K. P. (1996) *Annu. Rev. Biochem. 65*, 169−214.
2. Kornberg, A., and Baker, T. A. (1992) *DNA Replication* Freeman, San Francisco.
3. LeBowitz, J. H., and McMacken, R. (1986) *J. Biol. Chem. 261*, 4738−4748.
4. Baker, T. A., Funnel, B. E., and Kornberg, A. (1987) *J. Biol. Chem. 262*, 6877−6885.
5. Wickner, S., Wright, M., and Hurwitz, J. (1973) *Proc. Natl. Acad. Sci. U.S.A. 71*, 783−787.
6. Ueda, K., McMacken, R., and Kornberg, A. (1978) *J. Biol. Chem. 253*, 261−269.
7. McMacken, R., and Kornberg, A. (1977) *J. Biol. Chem. 253*, 3313−3319.
8. Bujalowski, W., Klonowska, M. M., and Jezewska, M. J. (1994) *J. Biol. Chem. 269*, 31350−31358.
9. Jezewska, M. J., and Bujalowski, W. (1996) *J. Biol. Chem. 271*, 4261−4265.
10. Jezewska, M. J., Kim, U.-S., and Bujalowski, W. (1996) *Biochemistry 35*, 2129−2145.
11. Jezewska, M. J., Kim, U.-S., and Bujalowski W. (1996) *Biophys. J. 71*, 2075−2086.
12. Jezewska, M. J., and Bujalowski, W (1996) *Biochemistry 35*, 2117−2128.
13. Dong, F., Gogol, E. P., and von Hippel, P. H. (1995) *J. Biol. Chem. 270*, 7462−7473.
14. Egelman, E. H., Yu, X., Wild, R., Hingorani, M. M., and Patel, S. S. (1995) *Proc. Natl. Acad. Sci. U.S.A. 92*, 3869−3873.
15. San Martin, M. C., Valpuesta, J. M., Stamford, N. P. J., Dixon, N. E., and Carazo, J. M. (1995) *J. Struct. Biol. 114*, 167−176.
16. Yu, X., Jezewska, M. J., Bujalowski, W., and Egelman, E. H. (1996) *J. Mol. Biol. 259*, 7−14.
17. Bujalowski, W., and Jezewska, M. J. (1995) *Biochemistry 34*, 8513−8519.
18. Jezewska, M. J., Rajendran S., and Bujalowski W. (1997) *Biochemistry 36*, 10320−10326.
19. Bujalowski, W., and Klonowska, M. M. (1993) *Biochemistry 32*, 5888−5900.
20. Bujalowski, W., and Klonowska, M. M. (1994) *Biochemistry 33*, 4682−4694.
21. Bujalowski, W., and Klonowska, M. M. (1994) *J. Biol. Chem. 269*, 31359−31371.
22. Secrist, J. A., Bario, J. R., Leonard, N. J., and Weber, G. (1972) *Biochemistry 11*, 3499−3506.
23. Cantor, C. R., Warshaw, M. M., and Shapiro, H. (1970) *Biopolymers 9*, 1059−1077.
24. Ledneva, R. K., Razjivin, A. P., Kost, A. A., and Bogdanov, A. A. (1977) *Nucleic Acids Res. 5*, 4226−4243.
25. Jezewska, M. J., and Bujalowski W. (1997) *Biophys. Chem. 64*, 253−269.
26. Lakowicz, J. R. (1983) *Principle of Fluorescence Spectroscopy*, Chapter 10, Plenum Press, New York.
27. Azumi, T., McGlynn, S. P. (1962) *J. Chem. Phys. 37*, 2413−2420.

28. Berman, H. A., Yguerabide, J., and Taylor, P. (1980) *Biochemistry 19*, 2226−2235.
29. Dale, R. E., Esinger, J., and Blumberg, W. E. (1979) *Biophysi. J. 26*, 161−194.
30. Nakayama, N., Arai, N., Bond, M., N., Kaziro, Y., and Arai, K. (1984) *J. Biol. Chem. 259*, 97−101.
31. Heyduk, T., and Lee, J. C. (1994) *Biochemistry 31*, 5165−5171.
32. Tolman, G. L., Barrio, J. R., and Leonard, N. J. (1974) *Biochemistry 13*, 4869−487.
33. Baker, B. M., Vanderkooi, J., and Kallenbach, N. R. (1978) *Biopolymers 17*, 1361−1375.
34. Cantor, C. R., and Pechukas, P. (1971) *Proc. Natl. Acad. Sci. U.S.A. 68*, 2099−2101.
35. Stasiak, A., Tsaneva, I. R., West, S. C., Benson, C. J. B., Yu, X., and Egelman, E. H. (1993) *Proc. Natl. Acad. Sci. U.S.A. 91*, 7618−7622.

BI972564U